

Department of Physics
Fisica Applicata FIS/07

“Bernardino Telesio”
“Doctorate School of Science and Technique”

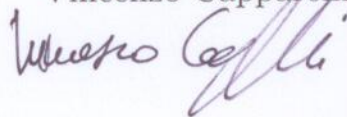
curriculum in “*Physics of Complex Systems*”

Cycle XXV

COMPLEXITY IN CLIMATE

PhD Candidate

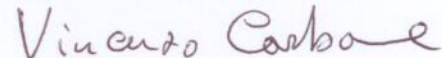
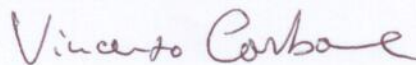
Vincenzo Capparelli



School Director
Prof. Roberto Bartolino

Curriculum Coordinator
Prof. Vincenzo Carbone

Supervisor
Prof. Vincenzo Carbone



2011 – 2012

Contents

Preface	1
Introduction	3
Climate system	4
Climate change and global warming	6
How to study the climate	6
1 The dynamics of seasonality	9
1.1 Introduction	9
1.2 Data Analysis	11
1.3 A simple model	18
1.4 Summary	21
2 Long-range persistence	25
2.1 Introduction	25
2.2 Data and methods	29
2.2.1 Definition of temperature anomalies	29
2.2.2 Analysis of persistence	34
2.3 Results	34
2.4 Summary	40
3 Temperature trends	43
3.1 Introduction	43
3.2 Methods	45
3.2.1 Temperature Data	45
3.2.2 Trend Identification	45
3.2.3 Statistical Significance Test	47
3.3 Results	49
3.3.1 Statistical significance of linear slopes	49
3.3.2 Nonlinear trend and local geographic parameters	53
3.4 Summary	55

4 Sun and oceans	57
4.1 Pair dispersion of photospheric bright points	57
4.1.1 Observations, analysis and results	58
4.2 Tsunami effects on Mediterranean	61
4.2.1 Data analysis and results	62
4.2.2 Summary	68
Appendix A	71
Empirical Mode Decomposition	71
Bibliography	75

Preface

This thesis is fruit of one's labours developed during my experience as Ph.D. student in physics of complex systems to Physics Department of University of Calabria and in collaboration with the British Antarctic Survey, one of the world's leading environmental research centres, where I spent six months of my life in the head office in Cambridge UK.

I am grateful to Professor Vincenzo Carbone for his steadfast attention to me. He was an excellent teacher and many discussion with him were an essential stimulus in a bad (scientific and not) moments. A special thanks to Dr. Antonio Vecchio for his many teachings, having endless patience to me.

The main topic of this thesis is a climate and its aspects as paradigmatic example of complex phenomena. Moreover related to global warming problem, climate dynamics turn out to be a field of research extended with remarkable implications on future of human life. Our approach at the problem was to investigate different climate effects (*e.g.* periodicity, randomness, trend) through analysis of historical geophysical parameters. The thesis is arranged as follow: in the introduction a short overview about the complexity and climate, in each chapter we describe and analyse a climate aspect separately. For this reason a section with general conclusion is not created, but in every chapter starts with a short introduction about the physical problem and it ends with a discussion and summary of obtained results

Introduction

The study of complex systems in a unified framework has become recognized in recent years as a new scientific discipline, the ultimate of interdisciplinary fields; in fact the field of study of complex systems holds that the dynamics of complex systems are founded on universal principles that may be used to describe disparate problems ranging from particle physics to the economics of societies (*Bar-Yam, 1997*). A dictionary definition of the word "complex" is: "consisting of interconnected or interwoven parts". To explain the difference between simple and complex systems, the terms "interconnected" or "interwoven" are somehow essential. Qualitatively, to understand the behaviour of a complex system we must understand not only the behaviour of the parts but how they act together to form the behaviour of the whole. It is because we cannot describe the whole without describing each part, and because each part must be described in relation to other parts, that complex systems are difficult to understand. This is relevant to another definition of "complex": "not easy to understand or analyse".



Climate system

In this thesis we focus our attention on the paradigmatic example related to complexity: the climate system.

Climate is a broad composite of the average condition of a region, measured by its temperature, amount of rainfall or snowfall, snow and ice cover, wind direction and strength, as well as other factors. Climate specifically applies to longer-term changes (years and longer), in contrast to the shorter fluctuations that last hours, days, or weeks and are referred to as weather. The Earth's climate system is an interconnected system formed by the atmosphere, the oceans and other bodies of water (the hydrosphere), land surface (the lithosphere), snow and ice cover (the cryosphere) as well as all living organisms (the biosphere), and powered by solar radiation. Beside its own internal dynamics, the system is affected by changes in external factors, which include natural phenomena such as solar variations and volcanic eruptions, as well as human-induced changes in atmospheric composition. At the most basic level, changes in these components through time are analysed in terms of cause and effect, or, in the words used by climate scientists, forcing and response. The term "forcing" refers to factors that drive or cause change; the responses are the climatic changes that result (*Bar-Yam, 1997*). Figure 1 provides an initial impression of the vast array of factors involved in studies of Earth's climate. It shows the major processes at work within the climate system, such as precipitation, evaporation, and winds. These processes extend from the warm tropics to the cold polar regions and from the Sun in outer space down into Earth's atmosphere, deep into its oceans, and even beneath its bedrock surface.

The complexity of the top part of Figure 1 is simplified in the bottom part to provide an idea of how the climate system works. The relatively small number of external factors shown on the bottom left force (or drive) changes in the climate system, and the internal components of the climate system respond by changing and interacting in many ways (bottom centre). The result of all these interactions is a number of observed variations in climate that can be measured (bottom right). A further factor capable of influencing climate, but not in a strict sense part of the natural climate system, is the effect of humans on climate, referred to as anthropogenic forcing. This forcing is an unintended by-product of agricultural, industrial, and other human activities, and it occurs mainly by way of additions to the atmosphere of materials such as carbon dioxide (CO_2) and other greenhouse gases.

From a physics point of view, climate dynamics is inherently complicated. The circulation of the atmosphere and oceans interact between phenomena on scales from centimetres to the globe and time-scales from seconds to millennia. As a mathematical tool to study the climate dynamics we have the fluids mechanical principles with complicated differential equations with the presence of non-linear terms with observed phenomena of air turbulence.

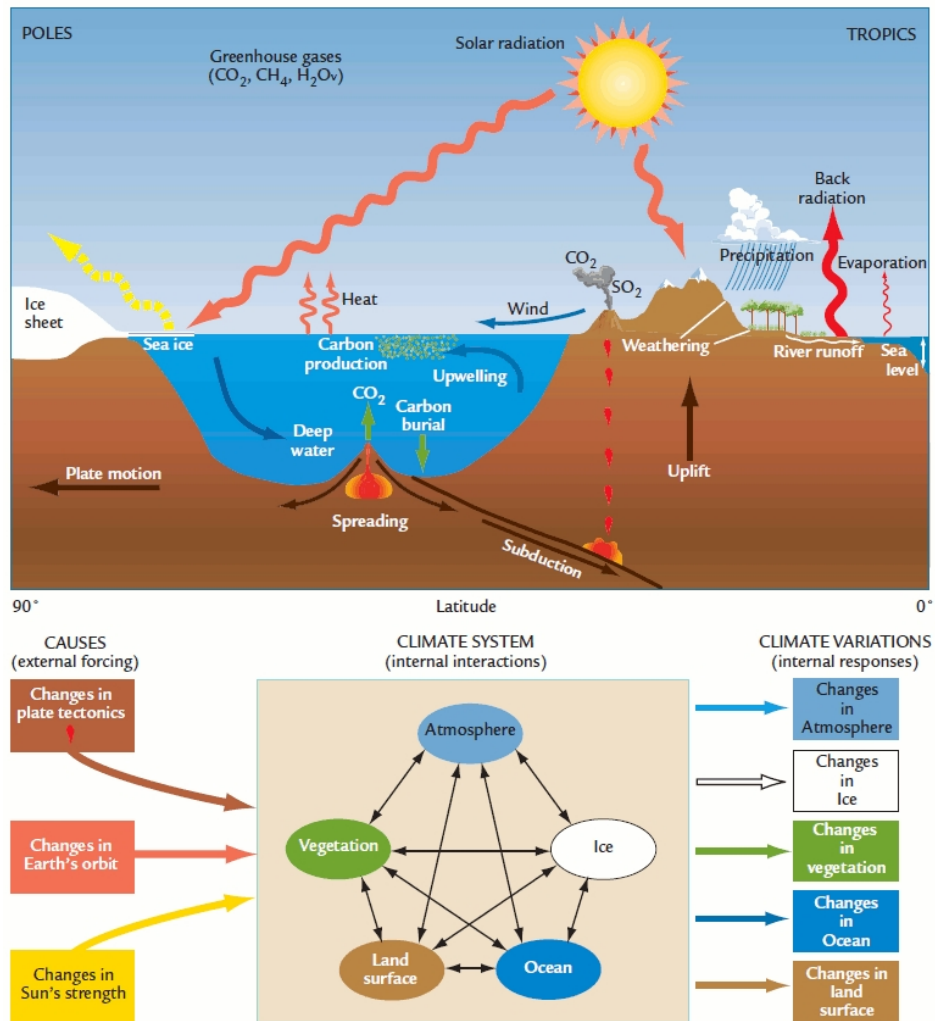


Figure 1: Earth's climate system and interactions of its components.

Climate change and global warming

Climate change is likely to be the predominant scientific, economic, political and moral issue of the 21st century (*Hansen and Sato*, 2012). By 2006, global climate had warmed by 0.7°C above the level in the late 1800s. Climate scientists agree that the atmospheric concentrations of CO₂ and other greenhouse gases produced by human activities have increased markedly in the last century, and they agree that the gas increases have caused climate to warm. The major disagreement over global warming has focused on whether the greenhouse-gas increases explain some, all, or little of the observed warming. During the several hundred years in which humans have been making scientific observations of climate, actual changes have been relatively small. Even so, climatic changes significant to human life have occurred. One striking example is the advances of valley glaciers that overran mountain farms and even some small villages in the European Alps and the mountains of Norway a few centuries ago because of a small cooling of climate. Scientific studies reveal that these historical changes in climate are tiny in comparison with the much larger changes that happened earlier in Earth's history. For these reasons in the last years a new line from Earth science was created, namely the Palaeoclimatology. It is the study of changes in climate taken on the scale of the entire history of Earth. It uses a variety of proxy methods from the Earth and life sciences to obtain data previously preserved within (*e.g.* rocks, sediments, ice sheets, tree rings, corals, shells and microfossils); Palaeoclimatology then uses these records to determine the past states of the Earth's various climate regions and its atmospheric system.

The debate about climate change and global warming related to human activity is still open, remembering that the fate of humanity and nature may depend upon early recognition and understanding of human-made effects on Earth's climate.

How to study the climate

Climate science moves forward by an interactive mix of observation and theory. Climate scientists gather and analyse data from the kinds of climatic archives and the results of this research are written up and published. Progress in science depends on the free exchange of ideas, and climate researchers publish in order to tell the scientific community what they have discovered.

These scientists interpret their research results and occasionally come up with a new hypothesis, an idea proposed as an explanation for observed data. A hypothesis that succeeds in explaining a wide array of observations over a period of time becomes a theory. Scientists continue to test theories by making additional observations, developing new techniques to analyse data, and devising models to simulate the operation of the climate system. Only

a few theories survive years of repeated testing. These are sometimes called "unifying theories" and are generally regarded as close approximations to "the truth," but the testing still continues.

Our Approach at the problem will be to study and investigate different climate phenomena through data analysis of historical geophysical parameters (*e.g.* temperature). Before we touched on the concept of complexity, namely a system with many interconnected or interwoven parts that interact together. In every chapter of this thesis we will be dealing of phenomenon with different characteristics between them. We start to observe and study in the first chapter the periodic dynamics of seasonality due to variation of temperature during the calendar year. In the second chapter we will be dealing about long-range predictably and random effects in a temperature records. The problem of trend and its definition will be discussed on third chapter using a spatio-temporal analysis of temperature trend rate in the last century. In the last chapter we will have two other geophysics complex phenomena, the first one related to Sun-Earth interaction and the second one the tidal level oscillation in Mediterranean sea.

Chapter 1

The dynamics of seasonality

The dynamics of the climate system has been investigated by analysing the complex seasonal oscillation of monthly averaged temperatures recorded at 1167 stations covering the whole USA. We found the presence of an orbit-climate relationship on time scales remarkably shorter than the Milankovitch period related to the nutational forcing. The relationship manifests itself through occasional destabilization of the phase of the seasonal component due to the local changing of balance between direct insolation and the net energy received by the Earth. Quite surprisingly, we found that the local intermittent dynamics is modulated by a periodic component of about 18.6 yr due to the nutation of the Earth, which represents the main modulation of the Earth's precession. The global effect in the last century results in a cumulative phase-shift of about 1.74 days towards earlier seasons, in agreement with the phase shift expected from the Earth's precession. The climate dynamics of the seasonal cycle can be described through a nonlinear circle-map, indicating that the destabilization process can be associated to intermittent transitions from quasi-periodicity to chaos.

1.1 Introduction

The annual rotation of the Earth around the Sun provides a quasi-periodic solar forcing that continuously synchronizes the terrestrial climate. The resulting seasons observed on Earth represent the complex nonlinear response of atmosphere, land and oceans to this forcing and are one of the most important source of variability for the climate system. In fact, even if climate changes are usually referred to trends in the average temperature records (*Alley et al.*, 2003; *Karl and Trenberth*, 2003), many studies have shown that the analysis on the seasonal cycle of the Earth temperature could improve our knowledge about climate changes (*Thomson*, 1995, 1997; *Huybers and Curry*, 2006; *Pez-zulli et al.*, 2005; *Stine et al.*, 2009). Unlike the external solar forcing, which is almost constant from year to year, there is no guarantee that climatic seasons

have to be the same each year. Actually seasonal variations cause more than 90% of the variance of a temperature record and represent one of the basic examples of the complex atmospheric response to external forcing (*Thomson, 1995, 1997; Mann and Park, 1996; Wallace and Osborn, 2002; Jones et al., 2003; Stine et al., 2009*).

At a given latitude the seasonal cycle is generated by the balance between two main components: i) the direct insolation component, which varies with the tropical year (the time from equinox to equinox) $\tau_{tr} \simeq 365.2422$ days; ii) a mean energy transport effect related to the net radiation received by the Earth, which follows the anomalistic year (the time from perihelion to perihelion) $\tau_{an} \simeq 365.2596$ days (*Thomson, 1995*). The seasonal cycle can be characterized by two quantities, namely amplitude and phase. While changes in amplitude are commonly interpreted as caused by stochastic climate fluctuations (*Huybers and Curry, 2006*) the phase of the seasonal cycle, namely the synchronization of each season during time, is yet poorly investigated. The variability of the seasons is not something new in climate research. For example, (*Cook et al., 2000*) pointed out that El Niño–Southern Oscillation (ENSO) has exhibited large changes in the amplitude and phase of the annual cycle as well as in the frequency/intensity of warm/cold events in the past century leading to inter-annual oscillations with multiple periods (*Jin et al., 1994; Jiang et al., 1995*). Previous studies about the phase of the global seasonality have underlined the presence of a phase shift.

Thompson showed that, after 1940, the phase behaviour started to change at an unprecedented rate with respect to the past 300 years (*Thomson, 1995*). Other authors indicated a global phase-shift towards earlier seasons (*Mann and Park, 1996; Wallace and Osborn, 2002; Jones et al., 2003*). A recent estimate (*Stine et al., 2009*) yields a global phase shift of the annual cycle of surface temperatures, over extra-tropical land between 1954 and 2007, of about $\Delta \simeq 1.7$ days. Even in this case the result seems to be highly anomalous with respect to the phase-shift of earlier periods.

The phase shift phenomenon has been attributed either to an increased temperature sensitivity to the anomalistic year forcing relative to the tropical year forcing due to Earth’s precession (*Thomson, 1995*), or changes in albedo, soil moisture and short-wave forcing, also involved in changing modes of atmospheric circulation (*Stine et al., 2009*). The anomalous phase shift recorded after 1940 has been attributed to the increasing presence of CO₂ in atmosphere (*Thomson, 1995; Stine et al., 2009*). The phase shift is not predicted by the current Intergovernmental Panel on Climate Change models (*Stine et al., 2009*), thus representing a yet rather obscure physical effect of the climate system. The role and exact extent of natural and anthropogenic forcing for the climate evolution has been under much debate (*Thomson, 1997; Keeling et al., 1996; Hasselmann, 1997; Rind, 2002; Alley et al., 2003; Karl and Trenberth, 2003; Scafetta and West, 2008*), and any attempt to point out

hidden aspects of climate dynamics is of considerable interest.

1.2 Data Analysis

In this section we focused on the phase of the seasonal oscillation by using an ensemble of temperature time series $T(t)$ from the United State Historical Climatology Network (the HCN data set is available at <http://cdiac.ornl.gov/epubs/ndp/ushcn/ushcn.html>). The data set covers 111 yr from 1898 up to 2008 and is recorded by $N=1167$ different stations distributed on the whole USA. The seasonal component has been identified through the Empirical Mode Decomposition (EMD) (see appendix). EMD decomposes the variance of each temperature record into a finite number of intrinsic mode functions (IMFs) and a residue, namely:

$$T(t) = \sum_{j=0}^{m-1} \theta_j(t) + r_m(t). \quad (1.1)$$

The intrinsic mode functions yield instantaneous phases $\Phi_j(t)$ and, after a time derivative, the instantaneous frequencies $\omega_j(t)$. For all records, the highest frequency IMF ($j=0$) represents the inter-seasonal stochastic component of the signal. High-order modes describe modulations of increasingly long periods, while the residue $r_m(t)$ represents the monotonically increasing local trend of temperature, commonly attributed to large scale warming since the urbanization contribution is smaller (see *Peterson, 2003; Parker, 2006; Jones et al., 2008*). The seasonal oscillation is described by the mode $j=1$ with a typical timescale of about $\Delta\tau_1 \simeq 1$ year. The statistical significance of information content for each IMF with respect to a white noise has been checked by applying the test developed by (*Wu and Huang, 2004*).

The 66% of the stations show an anomalous seasonal oscillation characterized by intermittent local decreases of the amplitude of the $j=1$ mode. For these stations the seasonal oscillation is spread over two EMD modes, namely the regular season is rediscovered when $\theta_1(t)$ and $\theta_2(t)$ are summed up. The remaining 34% of the stations shows a regular seasonal oscillation just isolated in the $j=1$ mode. An example from Evanston WY and Smithfield NC stations, characterized by regular and anomalous seasonal oscillation, respectively, is shown in Fig. 1.1 where the temperature records (panel a, b), the dynamics of $\theta_1(t)$ (panels c, d), the instantaneous Φ_1 (panels e, f) and unwrapped (panels g, h) phase, and the instantaneous frequency (panel i, j) are reported in a time interval of 30 yr. Each anomaly is associated with a strong variation of the instantaneous frequency and with an increasing phase-shift of the seasons, originating a destabilization of the phase Φ_1 of seasonal oscillation. This phase shift is marked by steps in the unwrapped phase plot (panel h). All these features are not observed for the “regular” station (left column

of Fig. 1.1). We have to remark that the amplitudes of the modes θ_1 are all above the 99% confidence level with respect to a white noise (*Wu and Huang, 2004*).

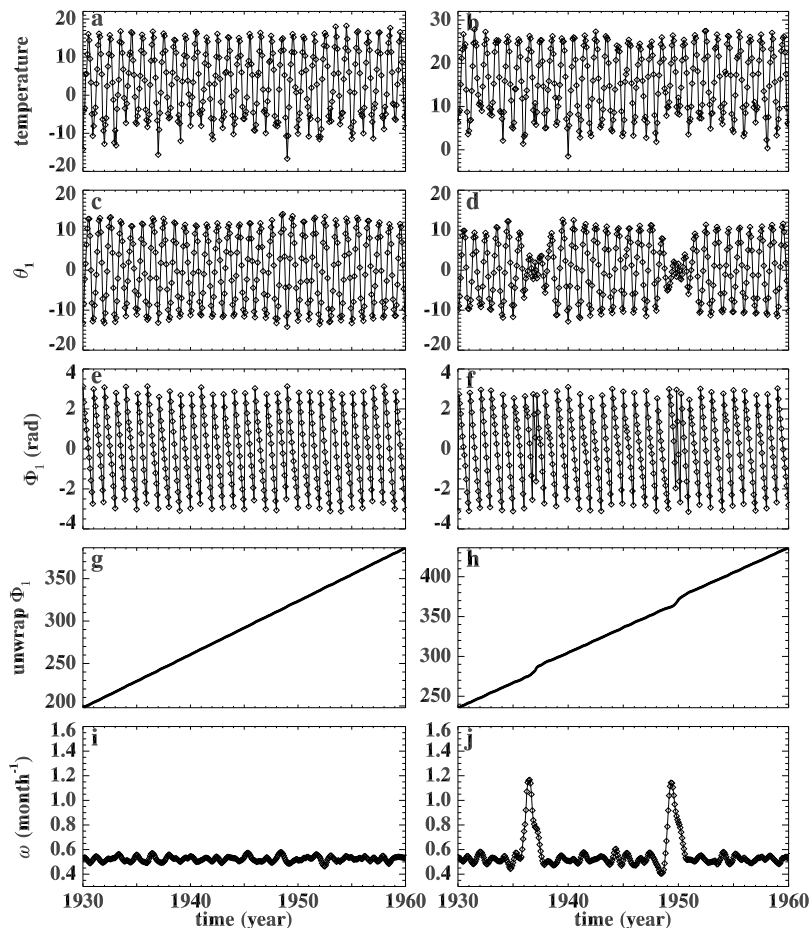


Figure 1.1: Examples of EMD results from Evanston WY record, characterized by regular seasonal oscillations, (left column) and from Smithfield NC, showing season anomalies (right column) in a 30 yr time interval. (a, b) refer to the rough data sets. The anomaly is underlined, in the right column, by the time evolution of: the IMF mode $\theta_1(t)$ (d), the phase $\Phi_1(t)$ (f), the unwrapped phase (h) and the instantaneous frequency (j). These quantities have been calculated by using the first EMD mode $j=1$.

In Fig. 1.2 the time evolution of the EMD modes $j=1$ and $j=2$ (panel a, b) and their sum (panel c) for the Smithfield NC temperature record is shown. The time behaviour of $\theta_1(t)$ is typical of the mode mixing effect, which makes a single IMF consist of signals of widely separated scales (*Huang et al., 1998*). This feature of EMD is troublesome in signal processing where the main pur-

pose is the signal cleanliness. In this framework, to effectively separate IMFs without mixed scales, the noise-assisted method named Ensemble EMD (*Wu and Huang, 2009*) has been developed. This approach consists in sifting an ensemble of white noise-added signal and treats the ensemble mean as the final true result. White noise series should cancel out in the averaging process, when a sufficient number of different realizations is used, thus reducing the chance of mode mixing. By using the EEMD (*Wu et al., 2008*) showed that the seasonal component of the analysed temperature record is also spread over two modes. Our analysis indicates a correspondence between phase anomalies and spreading of seasonal oscillations over two modes. Hence it seems very interesting to investigate the role of the phase intermittency in the temperature records and to relate it to the physics of the system. To this purpose the EEMD approach does not seem suitable, since it represents an ad hoc mechanism to cancel the intermittency from IMFs. On the contrary, if the goal of the research is to study the intermittency phenomenon in the analysed signals, then we need to analyse the IMFs as they are obtained by EMD. In this way an IMF, although affected by mode mixing, can be useful to identify when intermittency present. Moreover, because of their orthogonality, IMFs, differently from EEMD modes, can be given some more direct physical interpretation. The EMD is a technique developed to be highly sensitive to the local frequency (or phase, being $\omega = d\phi/dt$) fluctuations. For records showing irregular seasonal oscillations the frequency is slightly different from the expected one during an anomaly. In these cases, the detection of two IMFs, necessary to describe the full contribution of the season, results from the properties of the EMD decomposition for which each mode is associated to a well defined time scale. If a given time scale is present only during a small portion of the signal, namely Δt^* , the IMF describing this oscillation will be significantly different from zero only during Δt^* . The mode $j = 2$ simply provides the value of the "anomalous" frequency and the time intervals in which it occurs. The meaningful quantity is the sum $\theta_1 + \theta_2$ describing the full contribution of the seasonal cycle to the temperature record. In this application, the usefulness of EMD resides in its ability to highlight the periods in which the frequency of the season is anomalous. We have to remark that the EMD represents a powerful tool to deseasonalize the temperature record (see e.g. *Vecchio and Carbone, 2010*) by subtracting the reconstructed seasonality $\theta_1 + \theta_2$ from the raw record. This kind of approach is more efficient than the classical deseasonalization procedures involving time averages, since the temperature records are far to be stationary.

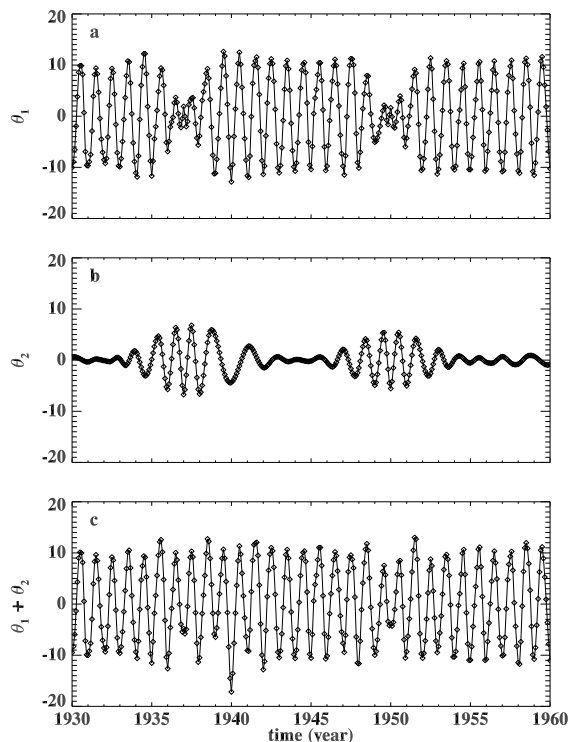


Figure 1.2: Time evolution of the EMD modes $j=1$ and $j=2$ (**a**, **b**) and their sum (**c**) for the temperature record in panel (b) of Fig. 1.1.

The analysis of the statistical properties of phase-shift events represents an important tool to characterize the nature of this outstanding phenomenon. By considering the anomaly occurrence as a point like process, that is, each of them is supposed to occur at its starting time t_i , we calculate the waiting time distribution (WTD), namely the probability density of the time intervals between two consecutive events $P(\Delta t)$. Quite interestingly the detected phase-shift events are strongly correlated in time. Two independent procedures have been developed to recognize the time of occurrence of a season anomaly:

1. since an anomaly corresponds to a strong local variation of the instantaneous frequency of the seasonal IMF, it can be identified with the formation of a spike in the local frequency (see Fig. 1.1 panel j). Since in principle positive and negative excursions in frequency can occur, the time of occurrence of each season anomaly corresponds to the local maximum in the range where the absolute value of instantaneous frequency is greater than two standard deviations of its average
2. anomaly occurrence is detected from the $j = 2$ IMF characterized by a temporal behaviour like those shown in Fig. 1.2 panel b. For this mode,

1.2 Data Analysis

the amplitude increases in correspondence of the season anomalies. The points of each interval where the absolute value of the amplitude exceeds two standard deviations of the chosen IMF are identified. For each interval the distance between extreme points, satisfying the previous threshold, defines the duration of the anomaly and identifies it.

The WTD calculated with the two different methods to identify anomalies, is shown in Fig. 1.3. An exponential shape of WTD corresponds to Poisson processes. In our case roughly equispaced peaks, superimposed to the exponential decay, can be recognized, thus indicating that the WTD is not associated to a stochastic process but there is a dominant periodicity. This is clear by looking at the binned occurrence of seasonal anomalies as a function of time (Fig. 1.4): phase-shift events show an oscillating behaviour. The main period P of the anomaly occurrence has been calculated through a sinusoidal fit over the red and black curve of Fig. 1.4, and by identifying the dominant peak in the Fourier periodogram (Fig. 1.5). The results are shown in table 1.1. The uncertainties have been calculated from the fitting procedure and from the Fourier period resolution at the found peak.

Table 1.1: Main period P of the anomalies occurrence calculated through a sinusoidal fit (first column) and from the dominant peak in the Fourier periodogram (second column).

	sin fit	Fourier
Method A	18.8 ± 0.4	20 ± 5
Method B	18.7 ± 0.2	18.5 ± 3.5

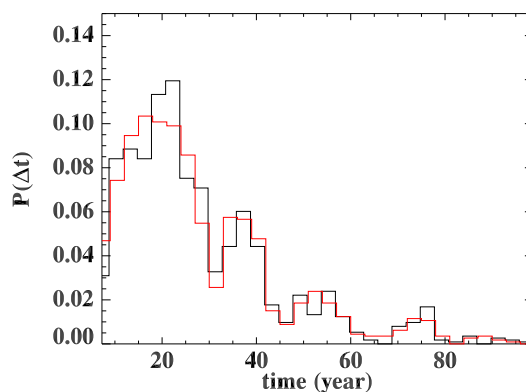


Figure 1.3: Waiting time distribution for the anomalies of seasonality for all the 1167 stations. Red and black curves refer to the different methods A. and B., described in the text, used to identify the anomalies.

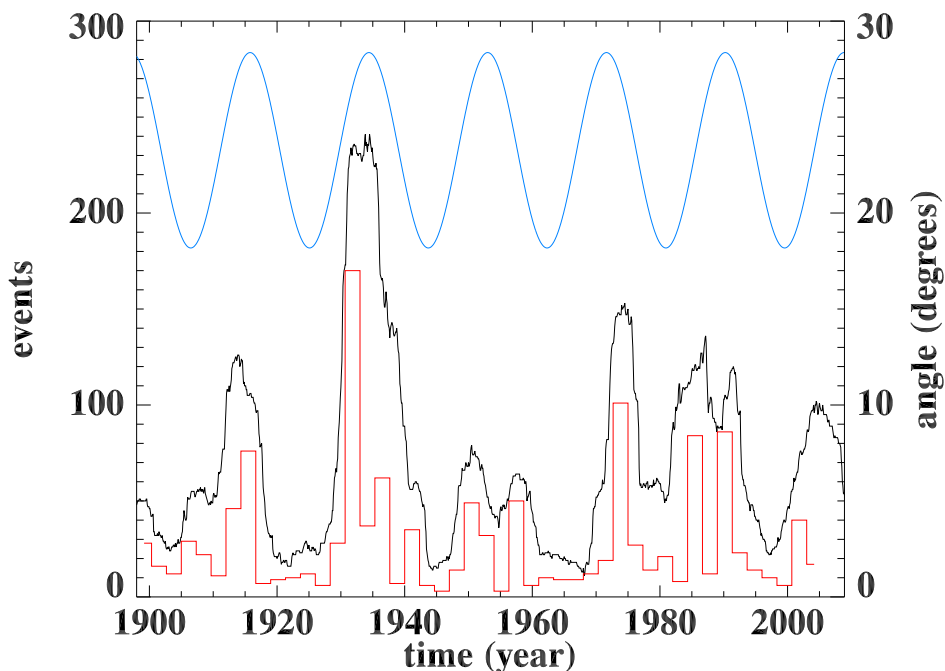


Figure 1.4: Anomaly occurrence detected in our dataset. Red and black curves refer to the methods A. and B., described in the text, used to identify the anomalies. The period of modulation, calculated for both curves, is reported in Table 1.1. The blue curve refers to the cycle of the changing inclination of the Moon’s orbit with respect to the equatorial plane due to nutation, modelled by $\psi=23^{\circ}27'+5^{\circ}09'\sin(\Omega_N t+\pi)$, where $\Omega_N=2\pi/18.6134\text{yr}$ (cf. *Yndestad*, 2006).

The value of the period P is remarkably close to the 18.6-year period of the Earth’s nutation, which represents the stronger modulation to the Earth’s precession. The same periodicity can be found in different geophysical phenomena connected with the Earth’s nutation (*Imbrie and Imbrie*, 1980; *Yndestad*, 2006). Figure 1.4 shows that, even if weak differences (e.g. the double peaked maxima around 1955 and 1990), the general trend of the periodic modulation of the anomaly’s occurrence is remarkably in phase with the inclination of the Moon’s orbit with respect to the Earth’s equatorial plane, all over the observation period, that is over at least six cycles. The linear Pearson’s correlation coefficient between occurrence of seasonal anomalies (black curve in Fig. 1.4) and the inclination of the Moon’s orbit (blue curve) assumes the value 0.57.

Since the phase-shift anomalies cannot be considered as purely stochastic events, we are going to discuss the origin of the above periodicity. We think this is a strong evidence of nutational forcing on temperature records probably due to an influence of the anomalistic year variability on seasonal timing variability (see *Thomson*, 1995). The amplitude and phase variability of cli-

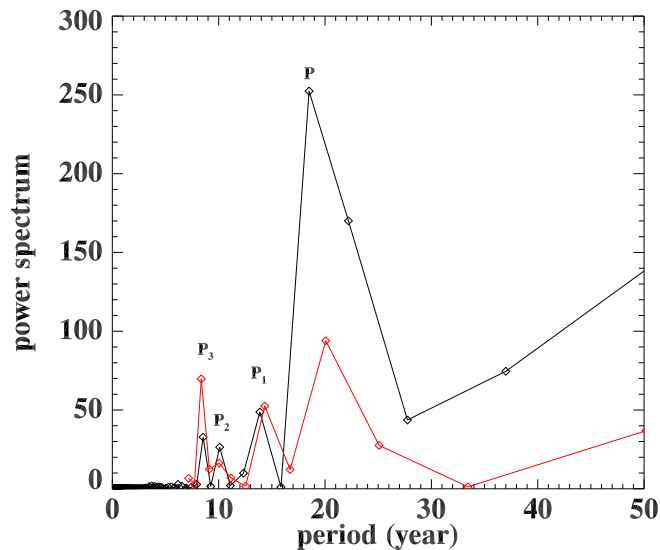


Figure 1.5: Fourier power spectra for the anomaly occurrence detected in our dataset. Red and black curves refer to the methods A. and B.

mate, which we call "season", is determined by the competing action of the direct insolation, having its maximum at the perihelion, and the net radiation received by the Earth, having its maximum at the summer solstice. In the Northern Hemisphere, summer solstice and perihelion are about 180° out of phase. Consequently, slight perturbation on either component can destabilize the system by changing the resultant proportionality. We can conjecture that the motion of the Earth's axis due to the nutation, by affecting the insolation, can continuously perturb the climate system. Due to strong nonlinearities in the atmospheric system, the climate response to the annual cycle of the solar forcing can be surprisingly abrupt, for example as it happens in the case of the rapid onset of the Asian monsoon (*Pezzulli et al.*, 2005). This coupling can generate impulsive destabilization of the phase which results in a global phase shift modulated by the nutation component. Being the temperature records strongly dependent on the local conditions, the nutation signal is detected only when a statistical analysis, over a significant number of stations, is performed. The above orbit-climate relation is amplified by the EMD, which is a technique extremely sensitive to the signal's phase shifts.

Three peaks, at low energy with respect to P , can be identified from the Fourier spectra of Fig. 1.5. They correspond to the periods $P_1 = 13.9 \pm 0.6$ yr, $P_2 = 10.1 \pm 0.8$ yr, $P_3 = 8.5 \pm 2.1$ yr. Similar periodicities have been found in previous works. In detail, P_1 is consistent with the ~ 15 yr periodicity in coastal surface air temperature in the Gulf of Alaska (GOA) (*Wilson et al.*, 2007) attributed to large-scale coherent Pacific climate variability. P_2 could be

related to the ~ 11 yr periodicity in ice core sequences (*Royer, 1993*) attributed to solar cycle effects. P_3 might be attributed to changing tidal current speeds due to interannual variability of the lunar orbit, in particular to the 8.85 yr period of rotation of the lunar perigee around the Earth (*McKinnell and Crawford, 2007*). It must be remarked that a periodicity of about 7.8 yr has been also found in drought data (*Cook et al., 1997*).

1.3 A simple model

To investigate the system response to the perturbation due to the nutation, the dynamics of the seasonal cycle has been described by the Phase Transition Curve (PTC), that is a basic tool to investigate recurrent dynamics as the time evolution of an oscillating system (e.g. *Arnold, 1965; Glass and Mackey, 1979; Croisier et al., 2009; Glass, 2001*). The PTC is a map describing the dynamics of an angular variable α_n , such that $\alpha_{n+1}=f(\alpha_n)$ where f is a given function. In our case the variable α_n is identified with $\Phi_1(t_n)$, namely the phase at a discrete time t_n ($n=0, 1, \dots$). A regular season is described by a linear map $\alpha_{n+1}=(\alpha_n+\omega_0)\text{mod}(2\pi)$, where ω_0 is the intrinsic frequency of the cycle. In Fig. 1.6 empirical PTCs are reported for the two stations of Fig. 1.1 (Evanston WY in panel a and Smithfield NC in panel b). In both cases, the dynamics of the PTC locally deviate from the linear behavior. For both maps the points are spread around the straight line, corresponding to the linear PTC, because of weak stochastic fluctuations due to random vagaries of the weather at monthly scales. Moreover, large excursions away from the linear dynamics are observed in panel b) in correspondence of the anomalies. The graphic iteration of this PTC map around a detected anomaly, from 1972 to 1975, is shown in panel c). Nonlinearities of the climate system, that is the occurrence of fluctuations which occasionally destabilize the system, cause significant deviations from the linear dynamics.

The observed PTC, including the effect of anomalies, can be reproduced by a so-called *circle map* (*Ott, 2002*), that describes the dynamics of a system characterized by two competing forcing with different frequencies. According to the general theory of dynamical systems (*Ott, 2002*), the circle map, in presence of two forcing oscillations, can be expressed in a linear form

$$\phi_{n+1} = (\phi_n + w)\text{mod}(2\pi) \quad (1.2)$$

where the winding number w corresponds to the ratio between the two competing frequencies. In our case $w=\tau_{\text{tr}}/\tau_{\text{an}}$ is the ratio between tropic and anomalistic year. When w is irrational the dynamics of the map is quasi-periodic, namely the orbit obtained from the iteration densely fills the circle as time goes to infinity (*Ott, 2002*). A nonlinear coupling between the external periodic forces is described by adding a function $f(\phi_n)$ to the right hand side of Eq. (1.2). The most famous example is the sine-circle map investigated by

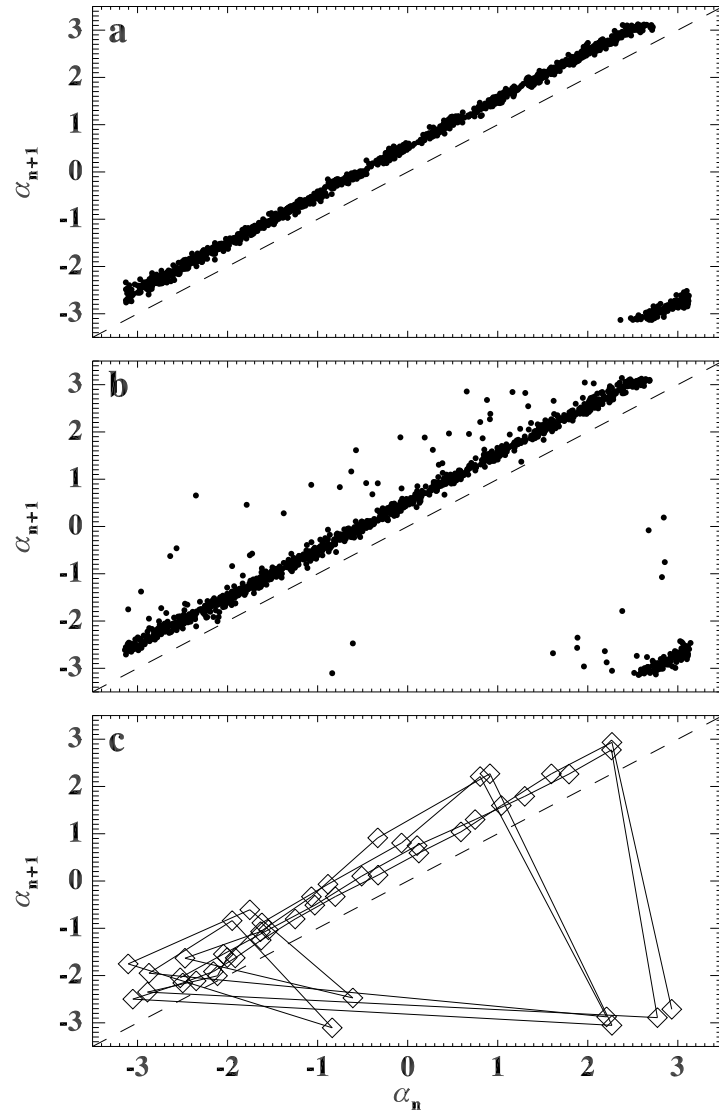


Figure 1.6: Phase Transition Curve $\alpha_{n+1} = f(\alpha_n)$ calculated using the data from Evanston WY (a) and from Smithfield NC (b) stations. An example of iteration of the panel (b) map around a given seasonal anomaly is reported in panel (c).

Arnolds

$$\phi_{n+1} = (\phi_n + w + k \sin \phi_n) \bmod(2\pi) \quad (1.3)$$

where k is a constant (*Arnold, 1965; Ott, 2002*). The presence of the nonlinear term destroys the quasi-periodicity in favour of the frequency locking because of the coupling thus generating an interesting transition to a chaotic state. Roughly speaking, the set of periodic points, which is of zero measure for $k=0$, increases as $k \neq 0$. For a fixed value of k , the rotation number

$$r = \frac{1}{2\pi} \lim_{N \rightarrow \infty} \sum_{n=1}^N (w + k \sin \phi_n) \quad (1.4)$$

as a function of w is an intricate sequence of periodic and quasi-periodic regions (*Ott, 2002*). Since in our case w changes because of the precession and nutation, the system moves into the net of periodic and quasi-periodic states and is continuously destabilized.

The empirical PTC (panel b in Fig. 1.6) indicates that during the seasonal anomalies the regular dynamics of the seasonal oscillation is destabilized. This can be described by conjecturing that the frequency locking phenomenon depends on the nonlinear coupling with the atmosphere. In order to reproduce our result we modify the sine-circle map by adding a periodic perturbation of the winding number and a variable coupling parameter k ,

$$\phi_{n+1} = [\phi_n + w + R_n + k_n(R_n) \sin \phi_n] \bmod(2\pi) \quad (1.5)$$

where the periodic term related to the nutation is $R_n = R_0 \cos(\Omega_N t_n)$ and the parameter $k(R_n)$ is not kept constant and represents the response to this perturbation. In particular, we conjecture that the response of climate to the orbit perturbation is a threshold phenomenon, so that the behavior of k can be described by the following map

$$k_{n+1} = \begin{cases} k_n & \text{if } R_n \leq R_{\text{th}} \\ z_n k_n (1 - k_n) & \text{if } R_n > R_{\text{th}} \end{cases} \quad (1.6)$$

where R_{th} is a threshold value. When the inclination of the Earth's axis is greater than a critical value, the frequency locking of the seasonal cycle occurs abruptly. This can be reproduced for example by a simple on-off intermittent process (*Platt et al., 1993*). In this framework the parameter z_n is suitably chosen to assume two values, say $z_n=1/2$ or $z_n=4$ with probability p and $(1-p)$, respectively. When $1/3 \leq p \leq 0.47$ the sequence of k_n behaves as a typical on-off intermittency (*Loreto et al., 1996*). Results of the model Eqs. (1.5) and (1.6), reported in Fig. 1.7, reproduce the observed behavior.

1.4 Summary

In this chapter we have shown the results of EMD to analyse the temperature records of 1167 stations, covering 111 yr, over the whole USA. Our results confirm that a complete study of the phase of the seasonal component of temperature records is fundamental to investigate climate changes. These are not simply related to trends in temperature records since even phase-shifts of the seasonal component seem to play an important role. We identify intermittent periods in most temperature records causing local events of phase shift. We assume that the climate system, usually lying in a quasi-periodic state, can be occasionally destabilized, due to unbalances between direct insolation and radiation received by the Earth generated by the nutation, re-synchronizing itself in a relatively small time. In other words, an increased sensitivity to the anomalistic year variability influences the seasonal variability. The phase shift occurrence, in fact, is modulated by an oscillating component whose period and phase are remarkably close to the Earth's nutation. The occurrence of local phase shifts causes significant deviations of the system from the linear dynamics since the response of the system to this kind of perturbations is highly nonlinear. Our findings represent an indication that the phase of the season is influenced by the Earth's nutation. The global phase shift, underlined by different authors in the past (*Thomson, 1995; Mann and Park, 1996; Wallace and Osborn, 2002; Jones et al., 2003; Stine et al., 2009*), could be related to the global effect of the local dynamics of impulsive phase-shift events. EMD results indicate that each anomaly of the seasonal cycle of temperature corresponds to a local phase shift well identified by steps in the unwrapped phase plots. By making use of simple statistical arguments we investigate if the combined effect of the anomalies could result in a global phase shift of the temperatures as detected by some authors (*Thomson, 1995; Mann and Park, 1996; Wallace and Osborn, 2002; Jones et al., 2003; Stine et al., 2009*). This can be quantified by looking at the probability distribution $P(\Omega)$ of $\Omega=w/\omega_0$ (Fig. 1.8), where $w=\lim_{n\rightarrow\infty}[(\phi_n-\phi_0)/2\pi n]$ is the theoretical winding number. Ω represents the phase shift with respect to the initial phase and it is normalized to the intrinsic frequency $\omega_0=2\pi/12$ months⁻¹, detected for each station from 1898 to 2008. Ω values different from 1 indicate a phase shift toward earlier, if $\Omega>1$, or later, if $\Omega<1$, seasons.

The Ω distribution is asymmetrical towards values greater than one, thus indicating an average shift towards earlier seasons. The maximum is found around the value $\Omega\simeq 1.03$ corresponding to a phase shift of about $\Delta\phi=|(1-\Omega)/\omega_0|\simeq 1.74$ days with a standard deviation of about 0.08 days. This result is in close agreement with the global shift estimated by (*Stine et al., 2009*). Thus the combined effect of the single phase shift on each station gives rise to a weak global phase shift of the seasonal cycle of surface temperatures of 1.74 days towards earlier seasons over 111 yr in agreement with past results.

We have to remark that the 18.6 yr periodicity has been found in other

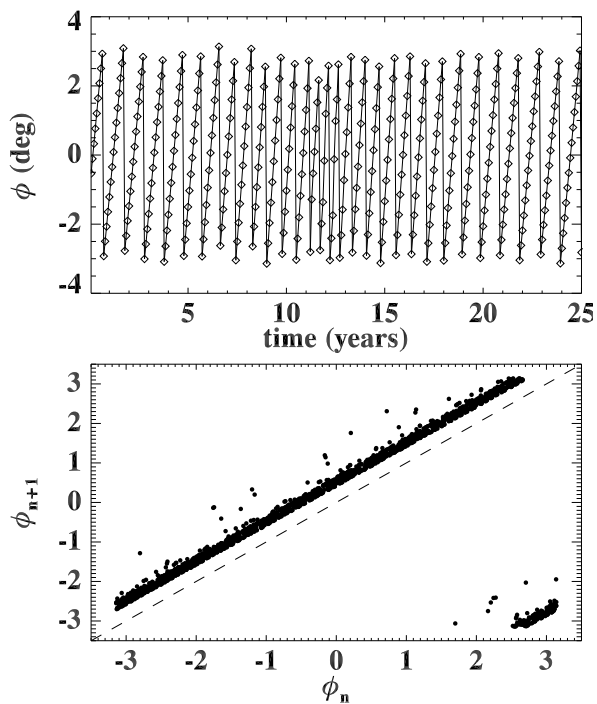


Figure 1.7: Results of the modified sine-circle map Eqs. (1.5) and (1.6) obtained with the following set of parameters (see text): $R_0=3\times 10^{-4}$, $R_{th}=2.6\times 10^{-4}$, and $p=0.43$. In the upper panel we report the behavior of ϕ_n around a given anomaly, while in the lower panel we report the Phase Transition Curve $\phi_{n+1}=f(\phi_n)$. Dashed line corresponds to $\phi_{n+1}=\phi_n$.

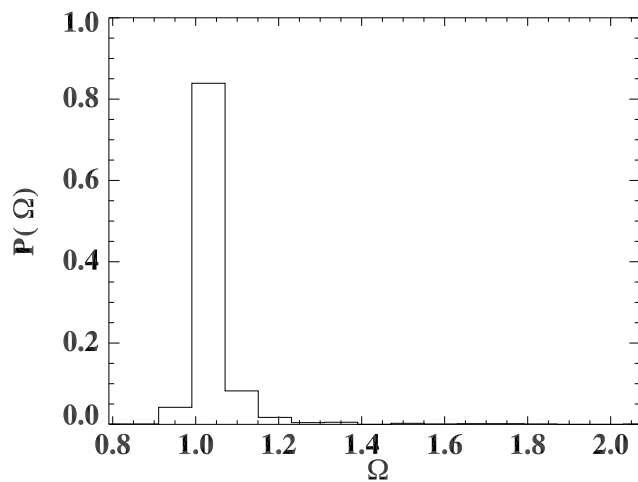


Figure 1.8: Probability of occurrence of the global phase-shift Ω normalized to the yearly seasonal frequency, calculated for all 111 yr of our dataset.

climatic time series like e.g, the air temperature and coastal sea surface temperature in the northeastern Pacific (*Royer, 1993; McKinnell and Crawford, 2007*), GOA coastal surface air temperatures (*Wilson et al., 2007*), drought occurrence (*Currie, 1984; Cook et al., 1997*), North Pacific Index and Pacific Decadal Oscillation Index (*Yasuda et al., 2006*) and have been commonly attributed to the external forcing of the lunar tides. Namely, the 18.6 yr luni-solar nodal cycle causes the long-term fluctuations of oceanic tides especially for the diurnal components. The high values of the tidal flow amplitude modulation, $\sim 20\%$, could affect the intermediate waters and large-scale oceanic circulation in the North Pacific. The coupling between bi-decadal variations in climatic data of northeast Pacific with the 18.6 yr nodal cycle has been modelled in terms of dissipation arising from local modulations of diapycnal mixing produced by the variable magnitude of diurnal tidal currents in the relatively shallow coastal ocean (*Yasuda et al., 2006; McKinnell and Crawford, 2007*). In other models, the bi-decadal fluctuation, interpreted by mid-latitude air-sea interactions with oceanic Rossby waves, has been obtained in a coupled ocean-atmosphere model and without the need for any external forcing (*Yasuda et al., 2006*).

It must be remarked that our model represents just a simple example to explain the observed behavior of the USA's temperature records, in terms of the variation of the insolation due to the nutation of the Earth. Previous papers, analysing different climatic datasets, do not clearly indicate whether the bi-decadal periodicity is related to the variation of the insolation due to the nutation of the Earth and/or lunar tidal forcing. This interesting topic will be the object of future investigations.

Chapter 2

Long-range persistence

Due to the nonlinear and nonstationary character of temperature time series, the seasonal cycle suffers for both phase and amplitude modulations, not properly removed by the classical definition of temperature anomaly. In order to properly filter out the seasonal component and the monotonic trends, we define in a new way the temperature anomalies by using the empirical mode decomposition (EMD). The original signal is decomposed into a collection of a finite and small number of intrinsic mode functions (IMF) and a residual, describing the mean trend (see appendix). The sum of all the IMF components as well as the residual reconstructs the original signal. Partial reconstruction can be achieved by selectively choosing IMFs in order to remove trivial trends and noise. The EMD description in terms of time-dependent amplitude and phase functions, overcomes one of the major limitation of the Fourier analysis, namely a correct description of nonlinearities and nonstationarities. By using the EMD definition of temperature anomalies we found persistence of fluctuations, with a different degree according to the geographical locations, on time scales in the range 3 – 15 years. The spatial distribution of the detrended fluctuation analysis exponent, used to quantify the degree of memory, indicates that the long term persistence could be related to the presence of climatic regions, which are more sensitive to climatic phenomena such as El Niño Southern Oscillation.

2.1 Introduction

The short term memory of many atmospheric parameters, due to the stochastic dynamics of atmosphere, is a well known phenomenon. This allows the predictability of the meteorological parameters over weekly time scales. The variability at low time scales has been traditionally described by low-order autoregressive processes whose paradigm is the first-order autoregressive process (AR1):

$$x_i = ax_{i-1} + \epsilon_i \quad (2.1)$$

where x_i is the meteorological variable at time t_i , a the first-order autocorrelation coefficient, and ϵ_i represents a Gaussian white noise. In particular, the parameter a introduces a rapid correlation decay so that the asymptotic behaviour, $x_i \sim \epsilon_i$, becomes uncorrelated and unpredictable starting from weekly scales. However, persistence has been found also at larger scales related to the occurrence of "red" noise in the power spectra of long-time meteorological records (*Ditlevsen et al.*, 1996; *Koscielny-Bunde et al.*, 1998; *Eichner et al.*, 2003; *Fraedrich and Blender*, 2003; *Govindan et al.*, 2002; *Syroka and Toumi*, 2001; *Király et al.*, 2006; *Vecchio and Carbone*, 2010). At these scales the presence of memory could be related to the slow response of e.g. oceans and ice cover or to climatic phenomena. For example, the weather is persistent when a very stable high pressure system is established over a particular region remaining in place for several weeks, the so called "blocking" (*Charney and Devore*, 1979). Persistence on monthly time scales has been related to slowly varying external forcing such as the sea surface temperature or intermittent phenomena in the solar-terrestrial system (*Eichner et al.*, 2003; *Scafetta and West*, 2003). The presence of memory in the system has been inferred by using the usual Detrended Fluctuation Analysis (DFA), obtained by investigating the scaling laws of fluctuations of detrended temperature anomalies, and in particular through a scaling exponent which indicate departures from a simple uncorrelated stochastic Brownian process (*Peng et al.*, 1994).

The Earth surface temperature represents one of the most analysed variable used to investigate the climatic system. Regarding the discussion of long range correlation in temperature time series some aspects remain still open. Firstly, *Koscielny-Bunde et al.* (*Koscielny-Bunde et al.*, 1998) proposed that the correlations should be universal, namely not dependent on the geographic location of the analysed station. The coupling of atmospheric and oceanic processes could be involved in setting of long-range persistence with the same exponent for the weather stations in different climatic zones and time regimes (from weeks to decades of years) (*Koscielny-Bunde et al.*, 1998). The effects of this coupling, in the context of interdecadal and century-scale climate oscillations (*Mann and Park*, 1996), is one of the core matter in climatology. More recently, the universality has been questioned since a wide range of exponent values seems to be present over continental lands (*Eichner et al.*, 2003; *Fraedrich and Blender*, 2003; *Kurnaz*, 2004) and marked differences seem to exist between land and sea surface temperature (*Fraedrich and Blender*, 2003; *Monetti et al.*, 2003; *Fraedrich et al.*, 2004). The latter has been attributed to slowly varying external forcing such as the presence of ocean or even big reservoirs of water (*Fraedrich and Blender*, 2003). On the basis of some detailed data analysis, it has been emphasized that the value of asymptotic power-law correlation exponent, obtained from usual datasets, is not constant but instead

depends on the scale (*Lanfredi et al.*, 2009). This apparent scale invariance has been described through a simple bivariate Markov model accounting for the fractal behaviour of the exponent (*Lanfredi et al.*, 2009). Because of these discordant evaluations, the claimed universality of persistence yet represents a matter of scientific debate (*Bunde et al.*, 2004; *Fraedrich and Blender*, 2010).

Another aspect depends on whether the universality is valid or not and concerns the geographic distribution of the correlation. In this regard, the analysis of Australian temperatures indicates that the intensity of the asymptotic correlation seems to decrease with the distance from the equator (*Király and János*, 2005). Analysis of more extended data set, acquired over the whole Earth, showed that correlations are grouped in large geographic areas which cannot be explained through a simple parametric dependence. In particular, the search for systematic dependence on the distance from the oceans gave negative results (*Eichner et al.*, 2003; *Király and János*, 2005; *Király et al.*, 2006), while controversial results have been obtained for a dependence on elevation for which both increase (*Efstathiou and Varotsos*, 2010), decrease (*Liu and Avissar*, 1999) and absence (*Király and János*, 2005) of correlation with the height have been found. Also, comparisons with global climate models lead to contrasting results. Seven state-of-the-art global models failed to reproduce the scaling behaviour of long temperature records by underestimating the long range correlation (*Govindan et al.*, 2002; *Syroka and Toumi*, 2001). A better model performance, regarding the possibility to reproduce long range correlations, can be obtained by properly taking into account the atmosphere-ocean coupling (*Fraedrich and Blender*, 2003) or by including volcanic forcing (*Vyushin et al.*, 2004).

We remark that the presence or absence of persistence represents a very useful test for the competing global climate models and to verify the basic assumptions underlying them (*Koscielny-Bunde et al.*, 1998) given that their reproductive power is an important request to interpret climate change predictions. Moreover investigation about the presence of memory in temperature records can contribute to the current debate over the global warming to distinguish the anthropogenic signal from the fluctuations due to the natural variability of the geophysical system (*Houghton*, 1995).

A key point in the calculation of the persistence concerns the presence of trends or trivial correlations in the raw temperature signal. In fact trivial correlations are introduced by the annual seasonal cycle, while long-term correlations can be masked by trends that can be generated by anthropic processes, e.g. the well-known urban warming, the increase of concentration of gases in atmosphere, etc. For these effect even uncorrelated data in the presence of long-term trends may look like correlated ones, and, on the other hand, long-term correlated data may look like uncorrelated data influenced by a trend. Usually, to remove trends and seasonal cycle the temperature anomalies are calculated. These are defined with respect to the seasonally varying mean

value. Namely, given a sequence of daily temperatures T_i , the anomalies ΔT_i are defined as the differences

$$\Delta T_i = T_i - \langle T_i \rangle \quad (2.2)$$

where $\langle T_i \rangle$ represents the temperature mean value for the i -th calendar day, averaged over a significantly large sample of data. Finally ΔT_i should account for the effect of long term climate change that should also be included in the definition of anomaly. The implicit assumption that the seasonal annual cycle is constant and is generated by a set of stationary processes underlies the definition (2.2). The validity of the previous assumption is often questionable due to the nonlinear response of the climate system to external forcing. Both trends or irregularities in the seasonal cycle have been observed as changes of both amplitude (*Wallace and Osborn, 2002*) and phases (*Thomson, 1995; Stine et al., 2009; Vecchio et al., 2010*) in the annual cycle of surface temperature. These effects are related to the complex nonlinear response of the atmosphere, land and oceans, to the periodic forcing provided by the annual motion of the Earth around the Sun (*Thomson, 1995; Vecchio et al., 2010*) or to changes in albedo, soil moisture and short-wave forcing (*Stine et al., 2009*). The presence of irregularities of the seasonal cycle, if not suitably filtered, can introduce a fictitious statistical randomization thus causing an artificial decrease of the persistence degree. Hence, because of the complex physics of the climatic system, the classical definition (2.2) average based of temperature anomaly could not be adequate and, as claimed by Thomson (*Thomson, 1995*) "Anomaly series used in climate research that have been deseasonalized by subtracting monthly averages need to be recomputed. The best method for doing this is not obvious". As a consequence, the persistence estimation calculated starting from the definition (2.2) might be misleading and might lead to introduce erroneous conclusions.

A different definition of temperature anomaly, based on the Empirical Mode Decomposition (EMD), should be more suitable to take into account the non-stationarities related to changes of amplitude and phase of the seasonal cycle (*Wu et al., 2008; Vecchio and Carbone, 2010*). In particular, when the DFA has been applied to very long European temperature records from Prague and Milan, very similar degree of persistence has been found, over a reduced range of scales (3 – 10 yr), by using a different definition of anomaly (*Vecchio and Carbone, 2010*).

In the present chapter we investigate the spatial distribution of the persistence degree of surface temperature in USA in order to discuss the claimed universality and for a better understanding of the physical processes responsible for long-term persistence in climate. In particular we compare the DFA results for temperature anomalies defined in the classical way (2.2) and through the EMD.

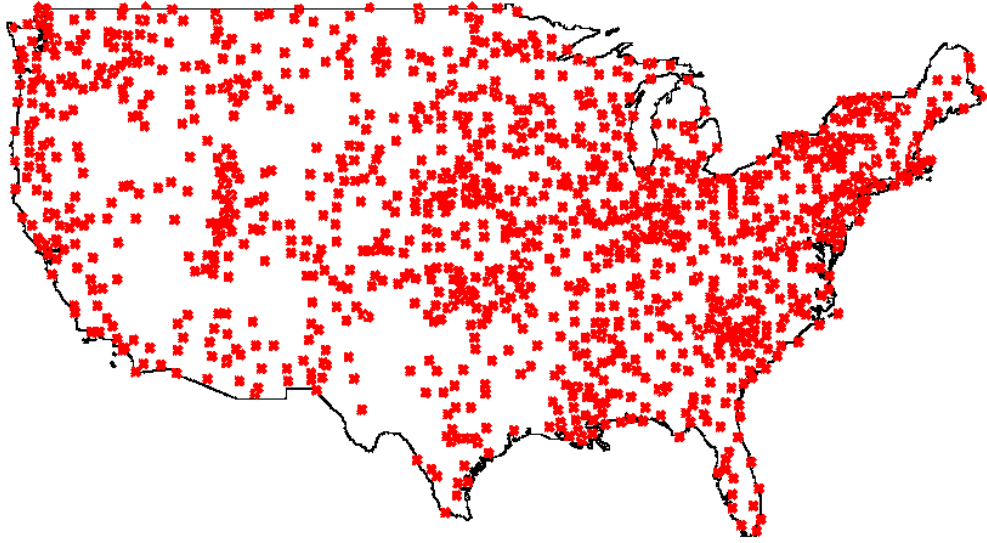


Figure 2.1: Spatial distribution of the stations.

2.2 Data and methods

We analyse the temperature records $T(t)$ from the United State Historical Climatology Network. The data set covers 111 years from 1898 up to 2008 and is recorded by $N = 1167$ different stations distributed on the whole USA. The N stations have been selected among other, in order to have homogeneous records characterized by the same duration and without gap. The spatial distribution of the N station over the USA is reported in figure 2.1.

2.2.1 Definition of temperature anomalies

The EMD approach is more appropriate when dealing with non-stationary and nonlinear data as temperature records. In these cases average operation, that critically depends on the chosen number of points, could cancel some of the relevant features in the original signal thus reducing temporal resolution. In the EMD framework (see appendix) a temperature record $T(t)$ is decomposed into a finite number n of Intrinsic Mode Functions (IMFs) as

$$T(t) = \sum_{j=0}^{n-1} \theta_j(t) + r_n(t) \quad (2.3)$$

The statistical significance of information content for each IMF, with respect to a white noise, can be checked by applying a specific test based on the following argument (*Wu and Huang, 2004*). When EMD is applied to a white noise series, the constancy of the product between the energy density of each IMF and its corresponding averaged period can be deduced. This relation can be used

to derive the analytical energy density spread function of each IMF as a function of different confidence levels. Thus, by comparing the energy density of the IMFs extracted from the actual data with the theoretical spread function, one can distinguish IMFs containing information at the selected confidence level from purely noisy modes. The temperature record filtered for trends and for the seasonal cycle, can be obtained by exploiting the orthogonality of EMD modes and reconstructing the signal through partial sums in (2.3) (*Huang et al.*, 1998; *Wu et al.*, 2008; *Vecchio et al.*, 2010). The orthogonality of IMFs guarantees that each j -mode captures a single aspect of the complex dynamics of the system. Thus it is meaningful to split the temperature signal in three part, namely a seasonal contribution $S(t)$, the anomaly $\Delta T(t)$ and the residual $r_n(t)$

$$T(t) = S(t) + \Delta T(t) + r_n(t) \quad (2.4)$$

For the analysed data set the residue $r_n(t)$ represents the monotonically increasing local trend of temperature, commonly attributed to large scale warming since the urbanization contribution is smaller.

By looking at the IMFs, identified by the index $j = 0, 1, \dots, n - 1$, we can define two mutually orthogonal sets of indices s and r , such that each $j \in s \oplus r$. Then, by partial sums, we can reconstruct the seasonal contribution by using only the subset s , that is:

$$S(t) = \sum_{j \in s} \theta_j(t) \quad (2.5)$$

while the remaining IMFs, belonging to the set r , are used to define temperature anomalies (*Vecchio and Carbone*, 2010)

$$\Delta T(t) = \sum_{j \in r} \theta_j(t) \quad (2.6)$$

Due to the complexity of the system, the sets r and s cannot be defined *a priori* rather they are suitably chosen by looking at the time behaviour of the various IMFs.

The EMD analysis on the monthly historical Prague and Milan temperature records (*Vecchio and Carbone*, 2010; *Vecchio et al.*, 2010) indicates that the the first IMF, $\theta_0(t)$, is associated to the weather vagaries at monthly scales, and the seasonal cycle for the Milan dataset is captured by the mode $\theta_1(t)$, characterized by a typical timescale of $\Delta\tau_1 \simeq 1$ yr. On the other hand, the seasonal cycle of the Prague dataset presents an irregular behaviour. In fact $\theta_1(t)$ show a regular seasonal oscillation interrupted by few intermittent local decreases of the amplitude and the full seasonal cycle is obtained when $\theta_1(t)$ and $\theta_2(t)$ are summed up. The same features are observed in the HCN USA data set analysed in this paper. Almost 66% of the stations presents an irregular seasonal cycle, while the remaining 34% of the stations shows a regular seasonal oscillation whose contribution is isolated in $\theta_1(t)$. As an example we report in Fig.2.2 the time behaviour of the mode $\theta_1(t)$ from both *Holly CO*

and *Covington LA* stations, which are characterized by regular and anomalous seasonal oscillations, respectively. In figure 2.3 the time evolution of $\theta_1(t)$ and $\theta_2(t)$ (panels a, b) and their sum (panel c), for the *Covington LA* temperature record, are shown over a restricted time interval of about 25 yr. As discussed in Ref. (Vecchio *et al.*, 2010) the seasonal irregularities, found in temperature records, do not occur randomly in time but their occurrence regularly oscillates with a period of 18.6 yr. Moreover, a strong phase coherence between the irregularity occurrence and the inclination of the Moon's orbit, with respect to the equatorial plane due to nutation, has been reported (Vecchio *et al.*, 2010). These observations indicate a possible connection between the Earth's nutation and the irregularities occurrence by means of modulation in the isolation and/or tides effects. We verified that the seasonal irregularities cannot be fully eliminated and the main results of this paper remain unchanged when the noise-assisted method named Ensemble EMD (EEMD) (Wu and Huang, 2009) is used. The latter has been developed, in signal processing, to achieve the signal cleanliness by removing irregularities thus obtaining regular modes. We remark that, in the case discussed in this paper, the EEMD approach does not seem suitable since the cancellation of the irregularities from IMFs could mask important physical aspects of the phenomenon at hand.

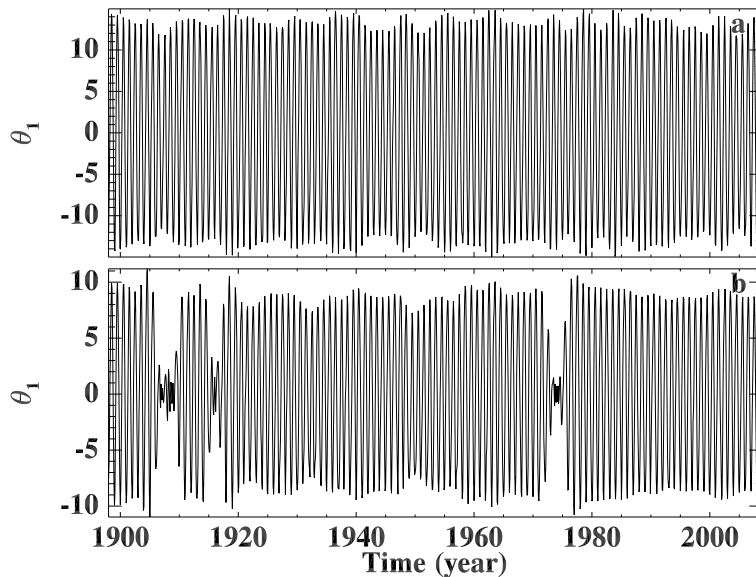


Figure 2.2: Time evolution of the EMD mode $j = 1$ and $j = 2$ for the temperature records *Holly CO* (a) and *Covington LA* (b).

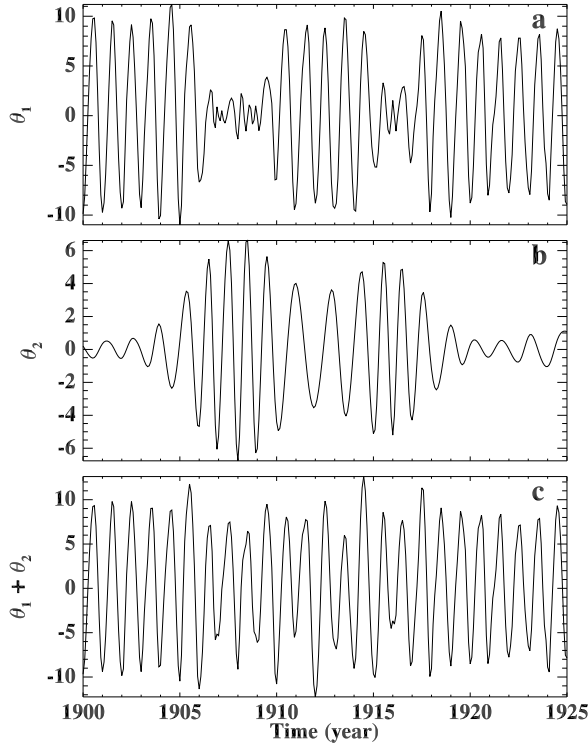


Figure 2.3: Time evolution of the EMD modes $j = 1$ and $j = 2$ (a, b) and their sum (c) for the temperature record *Covington LA*.

As far as the definition of temperature anomaly is concerned, the presence of irregularities in the seasonal cycle enforces the need for a new definition of anomaly. In fact non stationary periods, present in the temperature records, could affect the regular seasonal oscillation. Taking care of the above considerations, the most natural way to define temperature anomalies is to consider the contribution of all EMD modes but the properly defined seasonal oscillation. The latter contribution, as we said before, can be different according to the analysed record. Thus the set r in (2.6) represents the collection of EMD modes such that $r = \{j | 0 \leq j \leq n - 1\} \ominus \{j = 1\}$ in case of regular seasonal cycle (as for example in *Holly CO*), while $r = \{j | 0 \leq j \leq n - 1\} \ominus \{j = 1, 2\}$ in case of irregular seasonal cycle (as for example in *Covington LA*). With this choice the seasonal cycle, that could present amplitude and phase variations, is more properly excluded by the definition of temperature anomalies.

Fourier power spectra of $S(t)$ from *Holly CO* [Fig. 2.4 (c)] and *Covington LA* [Fig. 2.4 (d)] show the seasonal cycle isolated by the EMD. The Fourier spectra of $\Delta T(t)$ for both *Holly CO* and *Covington LA* records are reported in Figs. 2.4 (e) and 2.4 (f). Note that temperature anomalies defined through the EMD can be considered as deseasonalized at very good approximation.

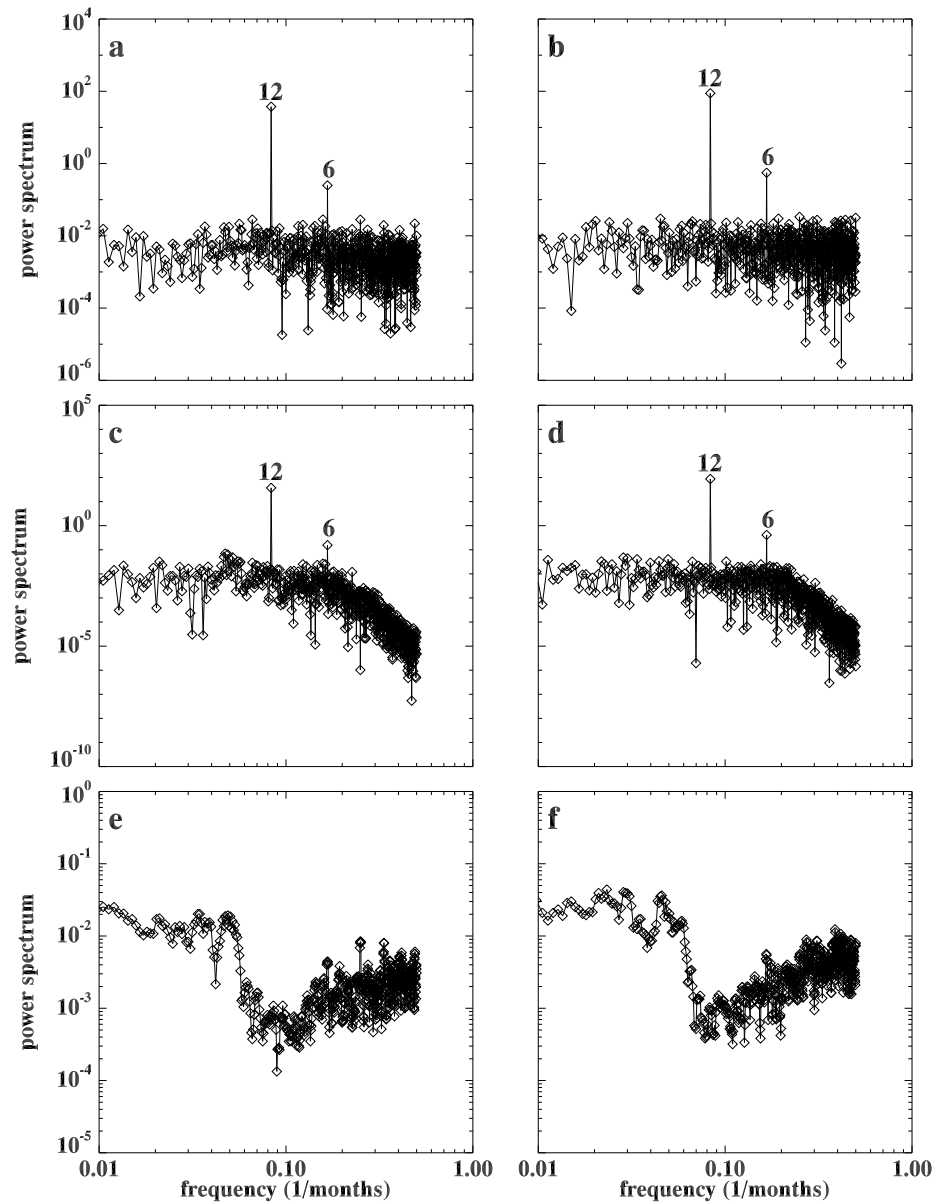


Figure 2.4: Upper panels report the Fourier power spectra of (a) *Holly CO* (a) and (b) *Covington LA* temperature records. Middle panels report the Fourier spectra of seasonal oscillation given by (c) the EMD mode $j = 1$ for *Holly CO* and (d) the sum of modes $j = 1$ and $j = 2$ for *Covington LA*. Lower panels represent the Fourier spectra of the temperature anomalies for both (e) *Holly CO* (e) and (f) *Covington LA*. The numbers over the peaks indicate the corresponding periodicity in months.

2.2.2 Analysis of persistence

To investigate the persistence in the analysed records, we used the Detrended Fluctuation Analysis (DFA) which consists of some standard steps. First of all from a sequence of anomalies of length N we extract y_k defined as:

$$y_k = \sum_{i=1}^k \Delta T_i . \quad (2.7)$$

y_k is then divided into boxes of equal time-length t_n and in each box a polynomial curve of order p is fitted, thus obtaining the local trend $y_k^p(t_n)$. The detrended signal $s_k^{(p)}(t_n) = y_k - y_k^p(t_n)$ is calculated for each box and the usual measure of fluctuation is given by the standard deviation of the detrended segment averaged over all the boxes

$$F_p(t_n) = \sqrt{\frac{1}{N} \sum_{k=1}^N [s_k^{(p)}(t_n)]^2} \quad (2.8)$$

A scaling exponent δ_p is then defined through the power law relationship $F_p(t_n) \sim t_n^{\delta_p}$. It can be shown that a process for which the power law relationship exists has also a power-law autocorrelation function $C(\tau) = \langle \Delta T_i \Delta T_{i+\tau} \rangle \sim \tau^{-\alpha}$ (where $0 < \alpha < 1$), and frequency spectrum given by $S(f) \sim f^{-\beta}$ (where $0 < \beta < 1$). The scaling exponents are related to the DFA index through $\alpha = 2(1 - \delta_p)$ and $\beta = 2\delta_p - 1$ (Koscielny-Bunde *et al.*, 1998; Talkner and Weber, 2000). Thus, a scaling exponent $\delta_p = 1/2$ is associated to uncorrelated Brownian-like stochastic processes, and separates a persistent process where $\delta_p > 1/2$ from an anti-persistent process where $\delta_p < 1/2$. According to previous analysis (Bunde *et al.*, 2004; Fraedrich and Blender, 2010; Király and János, 2005; Lanfredi *et al.*, 2009) we use the DFA2, namely $p = 2$ in (2.8). To reduce the noise level the standard "sliding window" technique, where local trend removal and variance computation were performed by choosing each possible starting values for a given box of length t_n , has been applied (Király and János, 2005).

2.3 Results

Since the stations we investigate cover the whole USA in a rather uniform way, we will focus on the spatial properties of the persistence and we discuss the differences obtained when the anomalies are defined in the classical way or through the EMD. The asymptotic DFA2 exponent can be used as a proxy for the presence of long-range effects not attributable to the intrinsic atmospheric fluctuations. In particular we fit the scaling relation $F_2(t_n) \sim t_n^{\delta_2}$ in the range of scales $3 \leq t_n \leq 15$ years. Such range has been chosen in order to directly

2.3 Results

compare our results with the cases studied in previous papers (*Fraedrich and Blender, 2010; Király and Jánosi, 2005; Vecchio and Carbone, 2010*). The uncertainties $\delta F_p(t_n)$ can be estimated from the uncertainties on $\delta s_k^{(p)}$, using definition (2.8), as

$$\delta F_p(t_n) = \frac{\delta s_k^{(p)}}{2\sqrt{F_p(t_n)}} \quad (2.9)$$

where $\delta s_k^{(p)}$ has been evaluated as the standard deviation of $[s_k^{(p)}(t_n)]^2$ over the boxes. When the anomalies are defined in the standard way (2.2), the χ^2 probability of the fit results below 0.6 for about 16% of stations, while this number increases to 37% when anomalies are calculated according to our definition through EMD. This means that, for some record, the accuracy of the fit is insufficient in the chosen range of scales, that is the persistence does not extend to longer periods. For these stations the accuracy level of the fit has been increased by reducing the upper value of t_n up to 7 years in order to reach an acceptably high accuracy (χ^2 probability ≥ 0.6) for all records. An example of the DFA2 curves for both *Holly CO* and *Covington LA* stations are shown in figure 2.5 where black and red lines refer to EMD and classically defined temperature anomaly, respectively.

The statistics of the DFA2 exponent is shown in figure 2.6, where the histograms of δ_2 (panel a) and its uncertainty $\Delta\delta_2$ (panel b) are reported for both definitions of anomalies. The values of δ_2 , for classical anomalies, are shifted toward lower values with respect to the persistence obtained when anomalies are defined through EMD. In particular, δ_2 values lower than 0.6 were detected for the 40% of stations, when anomalies are defined according to (2.2), while these values are detected in 16% of stations when EMD is used. The previous result indicates that the EMD reveals a long range positive correlation in the majority of USA. This means that the classical definition of temperature anomaly underestimates the degree of persistence, due to the randomization caused by stochastic fluctuations in the seasonal cycle which are not suitably filtered by the assumed constant seasonality in the classical definition. Both distribution of the uncertainties are sharply peaked around $\Delta\delta_2 \simeq 0.01$. We remark that this value is slightly lower than the error estimates performed by in the past (*Fraedrich and Blender, 2003; Király and Jánosi, 2005*) by using different approaches in the uncertainty evaluation.

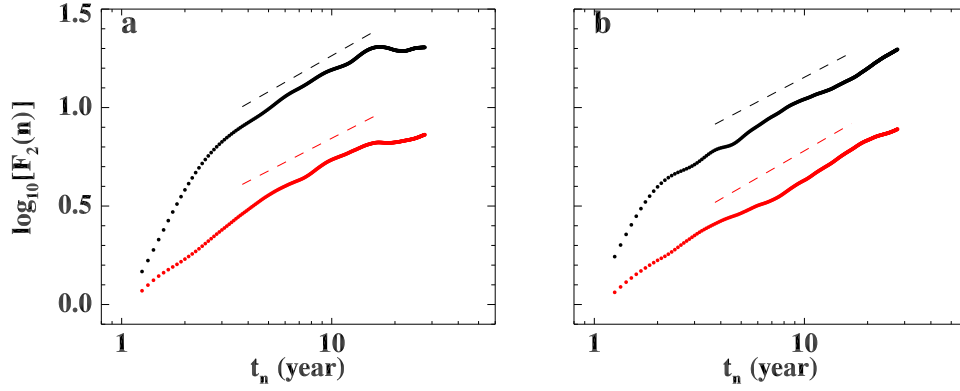


Figure 2.5: The scaling function $F_2(n)$ as a function of the temporal scale n for Holly CO (a) and Covington LA (b) stations. Black (upper) and red (lower) lines refer to EMD and classically defined temperature anomaly, respectively. Straight lines correspond to linear fits.

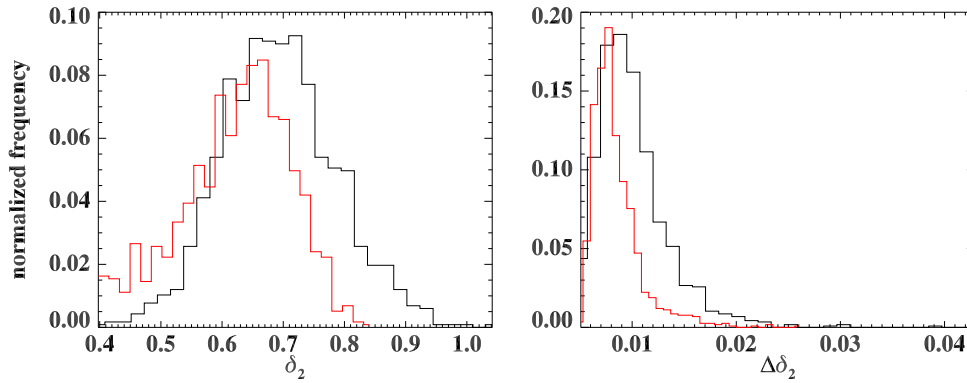


Figure 2.6: Normalized histogram of (a) DFA2 exponents and (b) their uncertainty calculated through the classical (thin red line) and EMD (thick black line) definition of temperature anomaly.

2.3 Results

A comparison between the geographic distribution of the DFA2 exponents is shown in figure 2.7 where the δ_2 maps are reported for both the anomalies defined in the classical way (panel a) and through the EMD (panel b). The maps has been built by computing the Voronoi polygon of each station, namely the polygon containing the region closer to that point than to any other point. Figure 2.7 clearly indicates that the correlation exponent is far from being universal in continental locations. For both maps the strength of long range correlation is distributed in large geographic patches, with substantial differences. In particular, panel a) shows two opposite patches of high and low degree of persistence. The first one is concentrated in the Rocky Mountains area where the height of the stations exceeds 1200 m. This results, however, should be not consistent with a linear dependence on the elevation since the correlation drops at the sea level while its maximum is located in a region where the average height of the stations is about 240 m (*Király and János, 2005*). The map reported in panel b) shows a more uniform distribution of the persistence index with higher values in two large areas, the first enclosed by the Atlantic ocean and the gulf of Mexico, namely the southeastern United States, and the second in the north-west part of the USA. We remark that the EMD identifies large values of persistence in the coastal areas, an expected results given the ocean's inertia. As in the map a), lower values of δ_2 are concentrated in the region of the Rocky Mountains. The latter result is in agreement with the findings of Ref. (*Weber and Talkner, 2001*) which show that the decorrelation of climate records is much stronger for the mountain stations. This effect could be due to the influence of the free atmospheric dynamic such as low-lying clouds and/or latent heat exchange of the surface (*Weber and Talkner, 2001*).

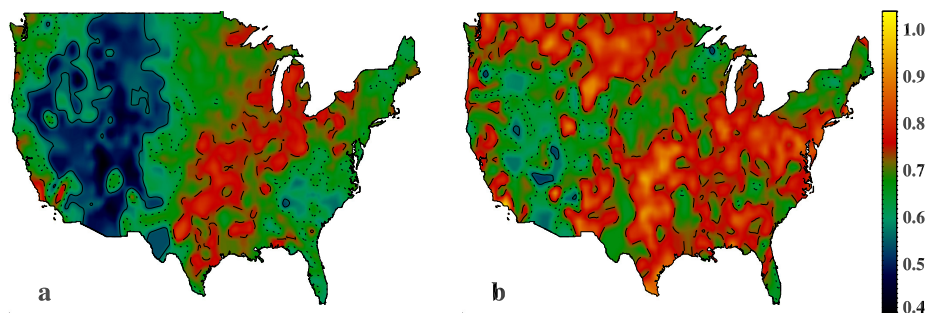


Figure 2.7: Geographic distribution of the DFA2 exponent δ of (a) classical and (b) EMD definition of temperature anomaly. Solid, dotted and dashed lines refer to levels 0.5, 0.6 and 0.7 respectively.

The pattern of persistence obtained from the classical anomaly is quite complex, it does not allow any simple correlation with long-term climatic phenomena and does not show a parameter dependence (e.g. distance from

oceans and/or elevation). On the other hand, the map obtained from the EMD anomaly allows an easier interpretation. In fact, we can recognize climatic regions through iso- δ_2 surfaces. In particular the observed spatial pattern suggests that the observed correlations in the temperatures could be induced by climatic phenomena. For example, it is well known that El Niño Southern Oscillation (ENSO) influences surface temperature at regional scales (*Ropelewski and Halpert, 1989; Halpert and Ropelewski, 1992*). The areas of high persistence values in the panel b) of figure 2.7, roughly correspond to the USA's regions showing a clearly defined (at the 99% significance level) ENSO-temperature relationship (see figure 8 from (*Ropelewski and Halpert, 1989*), figure 6 from (*Halpert and Ropelewski, 1992*)). The latter regions can be identified by using the method designed by Refs (*Ropelewski and Halpert, 1989; Halpert and Ropelewski, 1992*). In detail, monthly temperature composed, covering a two year interval including an ENSO episode, have been computed for all stations. For each temperature record 27 ENSO events, as identified from Refs (*Rasmusson and Carpenter, 1983*), have been considered. The first harmonic has been extracted from the 2 years temperature composed and its amplitude and phase have been calculated. Both these quantities, when plotted on the USA's map, indicate the magnitude and the phase of the response to the ENSO episode. A coherence map can be also built in order to underline the areas having a coherent response to the ENSO events. Figure 2.8 represents the normalized amplitude of the 24-months harmonic fit to the ENSO-temperature composed events. We remark that in the areas of high amplitude the coherence is greater than 0.9.

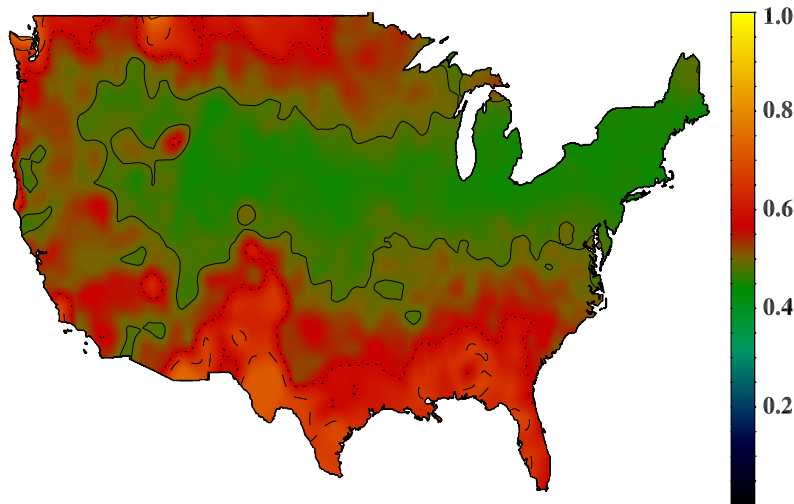


Figure 2.8: Normalized amplitude of the 24-month harmonic fit to the ENSO-temperature composed events (see the text for details). Solid, dotted and dashed lines refer to levels 0.5, 0.7 and 0.9 respectively.

Roughly speaking, figure 2.8 indicates the geographic areas in which the temperature records have a stronger and coherent ENSO response (*Ropelewski and Halpert, 1989; Halpert and Ropelewski, 1992*). A comparison between panel b) of figure 2.7 and figure 2.8 indicates that the areas of higher persistence values and higher temperature-ENSO response are similarly distributed in the southeastern and, mainly, in the northwestern United States. The temperature response to ENSO in North America can be related to the presence of tropical forcing of circulation pattern, in particular to the Pacific/North American (PNA) circulation pattern, induced by the forcing of the midlatitude circulation (*Ropelewski and Halpert, 1989*). Our result indicate that long-term persistence could be induced by ENSO on the surface temperatures, similarly to the relation between ENSO and sea surface temperature (*Monetti et al., 2003*). We remark that the presence of a persistence patch on the east-side in a narrow area enclosed between the Atlantic Ocean and the Great Lakes region not observed in the ENSO-temperature response map (figure 2.8). It could be related to the North Atlantic Oscillation (NAO), which represents one of the most prominent and recurrent patterns of atmospheric circulation variability driving decadal climate variability and trends from the eastern seaboard of USA to all Europe (*Hurrell et al., 2010*), and/or to the simultaneous neighbourly of the water reservoirs of the Great Lakes and Atlantic Ocean. The possibility to highlight a meaningful persistence pattern, possibly related to long-term climatic phenomena which induces correlations in the system, seems to be a prerogative of the EMD defined temperature anomalies. This could depends on the inadequacy of the classical definition of temperature anomaly in presence of quasiperiodic climate pattern, as the ENSO, whose signal could be aliased by the averages over the calendar day (*Halpert and Ropelewski, 1992*).

Other information are provided by the map in figure (2.9) showing the spatial distribution of the upper value of t_n chosen for the DFA fit so that the χ^2 probability exceeds 0.6, in the case of temperature anomaly defined through the EMD. Lower values are concentrated in a large area in the north-west and in smaller patches distributed in the south-east USA. The high values of persistence in the north-west are found in a narrow range of scales, namely $3 \leq t_n \leq 7$ yr, which also corresponds to the typical periods of the ENSO phenomenon. This represents a further indication that in this area the persistence could be related to the correlations induced by the ENSO. The south-east region, also characterized by high temperature-ENSO response, shows high persistence in a slightly large range of time-scales, namely $3 \leq t_n \leq 15$ years. This could indicate that the found correlations are related to other effects, such as the NAO or water reservoir due to the lakes and ocean, acting with the ENSO in this area.

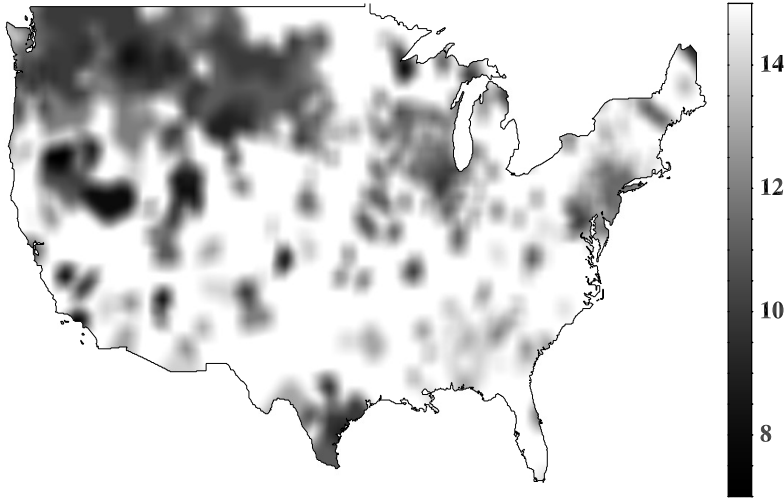


Figure 2.9: Geographic distribution of the upper t_n value, in year, used for the DFA fit, for temperature anomalies defined through the EMD.

2.4 Summary

In the present chapter we investigated the persistence of surface temperature anomalies within the USA. We introduced a different definition of temperature anomaly, based on the EMD orthogonal expansion of temperature records in empirical IMFs.

In fact, due to the presence of trends in the temperature records and phase-amplitude fluctuations in the seasonal component, the latter is badly filtered out when using the usual definition (2.2) of temperature anomalies (*Wu et al.*, 2008; *Vecchio et al.*, 2010; *Vecchio and Carbone*, 2010). On the other hand, the introduced temperature anomalies properly filter out a seasonal component which varies both in amplitude and phases. Spurious stochasticity introduced in the system by this effect is filtered out from temperature anomalies so that persistence can be properly calculated. The latter has been estimated through the DFA2 scaling exponent δ_2 which indicates departure from a Brownian memoryless stochastic process.

Temperature anomalies, defined through the EMD, show higher values with respect to δ_2 calculated through the classical definition of anomaly. We found that, long-term persistence clearly exists at timescales in the range $3 \leq t_n \leq 15$ years with a different degree of persistence according to the geographical locations. The proper definition of anomalies allows to a better estimate of errors in the calculation of persistence. In fact, the uncertainty associated to the scaling exponents δ_2 , calculated in a statistical way during the DFA computation, is lower than the error estimates discussed in literature (*Fraedrich and Blender*, 2003; *Király and Jánosi*, 2005).

2.4 Summary

Our analysis indicates that the long term persistence can be related to the regional effect of climatic phenomena. In fact, the spatial pattern of the scaling exponents, obtained by using the EMD definition of temperature anomalies, reflects the areas showing stronger ENSO-temperature relationship. By reversing the point of view, the spatial distribution of the persistence degree provides a quantitative way to discriminate among the different climatic regions. To this purpose, the areas of higher persistence in panel b of figure 2.7, appear similar to the climate zones of the USA (lower map at <http://www.eia.gov/consumption/residential/methodology/index.cfm>). It is well known that decadal climatic phenomena, as the ENSO, influence surface temperatures in the south-east and north-west part (*Ropelewski and Halpert, 1989; Halpert and Ropelewski, 1992*) of USA. We found that the north-west region manifests a strong persistence in the range of scales $3 \leq t_n \leq 7$ years, namely the typical time scales of the ENSO. The south-east regions manifest persistence over a slightly greater range of scales, namely at $3 \leq t_n \leq 15$ years. This indicates that in the latter regions other effects, such as the NAO or water reservoir, could operate with the ENSO in inducing correlations. The results obtained when EMD-defined temperature anomalies are used, e.g the presence of a meaningful persistence spatial pattern, depends on the estimate of the temperature anomalies, where amplitude-phase modulated seasonal component and the local trends can be suitably removed, thus not masking the presence of long-term climatic phenomena which induces persistence.

Chapter 3

Temperature trends

This chapter presents a nonlinear spatio-temporal analysis of 1167 station temperature trend covering the period from 1898 through 2008. We use the Empirical Mode Decomposition (EMD) method (see appendix) to extract the generally nonlinear trends of each station. The statistical significance of each trend is assessed against three null models of the background climate variability, represented by stochastic processes of increasing temporal correlation length. We find strong evidence that more than 50 percent of all stations experienced a significant trend over the last century with respect to all three null models. A spatio-temporal analysis reveals a significant cooling trend in the South-East and significant warming trends in the rest of the contiguous US. It also shows that the warming trend appears to have migrated equatorward and possibly also in altitude. This shows the complex spatio-temporal evolution of climate change at local scales.

3.1 Introduction

Changes in climate have significant implications for societies, future generations, the economy, ecosystems and agriculture. Consequently, climate change, and especially its anthropogenic forcing, has been, and continues to be, the subject of intensive scientific research and public debate (*The Royal Society*, 2010). Due to the complex nature of climate dynamics, understanding the response of the climate system to different forcings is a challenging problem, involving analysis of the variations and trends in long time series of atmospheric measurements and proxy records. The global mean surface air temperature is one of the most important and most discussed indicators of global change. It has risen by about 0.5°C during the 20th century and been attributed (mostly) to a rise in greenhouse gases (*IPCC*, 2001).

While global mean temperature is a useful indicator of global climate change, many policy makers and the general public are more interested in whether they already feel the effects of global warming where they live. Be-

cause the background climate variability plays a much larger role on smaller spatial scales than for the global mean (*Hawkins and Sutton, 2009*), local and regional temperature trends are easily masked by natural temperature fluctuations and their identification is further complicated by the fact that climate change is not happening in general in a monotonic and uniform way (*Wu et al., 2007*).

The term trend is frequently encountered in data analysis and is one of the most critical quantities in global change research. For example, in a casual Internet search, there are presently more than 12 million items related to trend and detrending (*Wu et al., 2007*). Thus, different techniques have been used to identify a trend because there is no general definition of what a trend should be (*Wu et al., 2007; Franzke, 2009*) and so in general a trend depends on the method one is using to identify it. The simplest definition of a trend, and the one most often used in climate research, is a straight line fitted to the data. But this may be illogical and physically meaningless in the real nonlinear and non-stationary world (*Wu et al., 2007; Franzke, 2009*). Another definition of trend is a running mean of the data, which requires a predetermined time scale to carry out the smoothing operation. This has little rational basis, since in a stochastic or chaotic non-stationary process the local time scale is unknown *a priori* (*Wu et al., 2007*). More complicated trend extraction methods, such as regression analysis or Fourier-based filtering, are often based on stationarity and linearity assumptions and thus face a similar difficulty in justifying their usage (*Wu et al., 2007*). Since the trend of the data should be an intrinsic property of the data, the processes of determining the trend have to be adaptive to accommodate data from non-stationary and nonlinear processes. The recently developed Empirical Mode Decomposition (EMD) method (see appendix) fits these requirements.

Fundamentally, climate change science concerns the identification and understanding of climate trends caused by changing external physical processes. However, it is complicated by the fact that the climate system is a complex system in which a large number of processes nonlinearly interact with each other to produce variations over vastly different time and space scales. Thus even a stationary climate system will create apparent, so-called stochastic, trends over rather long periods of time, which need to be distinguished from that of a non-stationary external influence (*Fatichi et al., 2009; Barbosa, 2011; Franzke, 2009, 2010, 2012*).

In order to do this, it is usual to compare the observed trend with the statistical distribution of possible trends from a simple stochastic null model. The most widely used null models in climatic trend analysis are Gaussian white noise (e.g., (*Wu et al., 2007*)) or an autoregressive process of first order (AR(1), e.g., (*Santer et al., 2000, 2008; Franzke, 2009*)). These two are so-called short-range dependent processes. However, there is increasing evidence that the climate system is long-range serially correlated, unlike white noise, and over

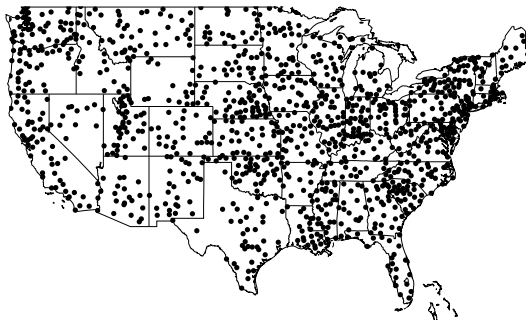


Figure 3.1: Geographic distribution of the 1167 stations.

a longer range than AR(1) (e.g. (*Huybers and Curry, 2006; Koscielny-Bunde et al., 1998; Franzke, 2010*)). For this reason we will also use a long-range dependent process in our trend analysis.

In the present chapter we study the statistical properties of nonlinear annual mean local temperature trends from 1167 stations covering the 48 geographically contiguous states of the USA for the period 1898 through 2008. A previous study by (*Lu et al., 2005*) analysed an earlier version of this data set covering a shorter time period and less stations. They also tested the significance of the linear trends against a periodic autoregressive moving average process. Here we will use the updated version of this data set and test the significance of the trends against three different null models of varying correlation length and also use a nonlinear and non-stationary method to identify the trends.

3.2 Methods

3.2.1 Temperature Data

In this study we analyse the trends of temperature times series at individual stations from the United States Historical Climatology Network (*Menne et al., 2009*) (the data are available at <http://cdiac.ornl.gov/epubs/ndp/ushcn/ushcn.html>). The data set covers 111 yr from 1898 up to 2008 and consists of 1167 different stations in the 48 contiguous states of the USA (Fig. 3.1). The data are homogenized, have no breaks, and the urbanization effect is likely small (*Menne et al., 2009*).

3.2.2 Trend Identification

The trends are identified through the Empirical Mode Decomposition (EMD) technique, developed to process nonlinear and non-stationary data (*Huang et al., 1998*) and successfully applied in many different fields (*Loh et al., 2001*;

Echeverria et al., 2001; *Coughlin et al.*, 2004; *Vecchio et al.*, 2010; *Laurenza et al.*, 2012; *Capparelli et al.*, 2011). EMD decomposes a time series into a finite number of intrinsic mode functions (IMFs) and a residual (see appendix):

$$T(t) = \sum_{j=0}^{m-1} \theta_j(t) + r_m(t). \quad (3.1)$$

In this study we define this residual as the EMD trend.

As shown by (*Wu et al.*, 2007), the IMFs and the residual obtained by using EMD can depend on the stopping criterion for the sifting process. The ambiguity depends on the dataset and in particular on the sampling rate. In a temperature record the main modulations are the daily oscillation (due to the difference of temperature from day to night) and the annual oscillation (due to seasonality). If we apply the EMD decomposition on temperature time series with a sampling rate less than one year then a single IMF mode will turn out to be dominant compared to the rest of the IMF modes (*Vecchio et al.*, 2010), making the iteration to identify the EMD residual very sensitive to the sifting conditions. For this reason we decided to use the annual mean of the temperature time series for each station. Using these data we verified that for all stations the shape of the residuals $r_m(t)$ does not depend on the value of σ_{thr} selected.

The complexity of the definition of a trend can be seen in fig. 3.2, where we show an example of the annual mean temperature time series of the station Highland (Alabama). A linear least square fit to the raw data reveals an overall secular decrease with a slope of $m_{raw} = (-0.986 \pm 0.172)^\circ\text{C}/\text{century}$, which is statistically significant with respect to the null hypothesis of a white noise times series with no trend. However, the residual $r_m(t)$ of the EMD analysis is a nonlinear function of time, implying the existence of a "nonlinear trend". While a linear fit of the residual function $r_m(t)$ gives the linear slope $m_{EMD} = (-1.185 \pm 0.046)^\circ\text{C}/\text{century}$, which is compatible with m_{raw} , the occurrence of a nonlinear trend function implies different physical and practical interpretations with respect to the linear model, with local acceleration and deceleration of the average mean temperature.

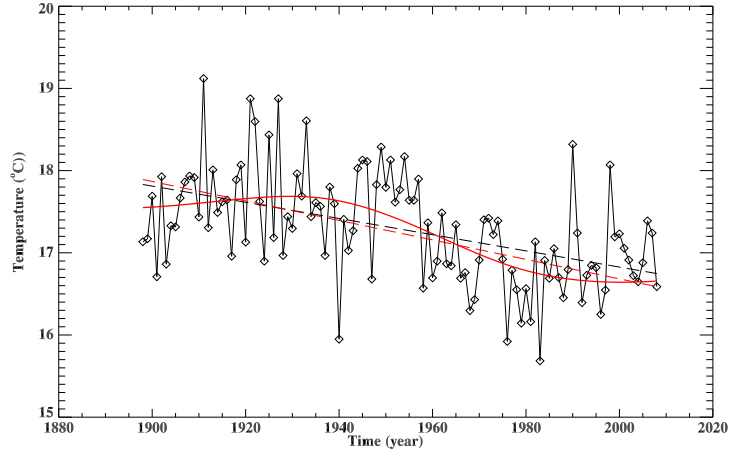


Figure 3.2: Annual mean temperature record for the station of Highland, Alabama. The EMD trend is the solid red line, while the dashed lines denote the linear least square fits to the raw data (black) and the EMD trend (red).

3.2.3 Statistical Significance Test

In order to illustrate the fact that the stations experienced significant variability on many time scales we first consider the variance of each IMF with respect to a simple white noise model. Following the arguments of (*Wu and Huang, 2004*), Figure 3.3 shows the theoretical spread function (dashed line) of the logarithm of the variance and the logarithm of the averaged period obtained from a white noise process using a 95% confidence level. This is compared with (diamonds) the relationship associated with each $\theta_j(t)$ and $r_m(t)$ for the representative station of Highland (Alabama). This analysis shows that this station experiences variability on many time scales which are different from the simple uncorrelated noise model because the variances of the IMFs are well above of the 95% spread function curve. In addition, note that the observed trend is significant at the 95% level and thus unlikely to be due to the intrinsic fluctuations of this simple null model of the background climate variability.

Thus, we use three different paradigmatic null models with increasing correlation length to test the significance of the observed trends: (i) Gaussian white noise, (ii) short-range dependent (SRD) and (iii) long-range dependent (LRD). As the SRD model we use an AR(1) process (*von Storch and Zwiers, 1999*). As the LRD model we use an autoregressive fractional integrated moving average process (ARFIMA (*Hosking, 1981; Robinson, 2003; Stoev and Taqqu, 2004; Franzke et al., 2012*)).

To systematically assess the significance of trends we use the following approach for each station:

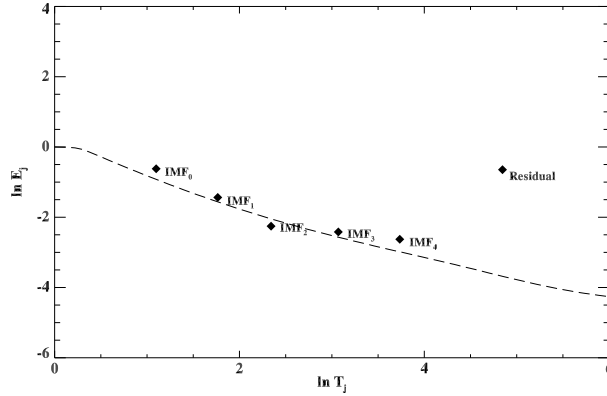


Figure 3.3: Statistical significance test for the annual mean temperature record for the Highland, Alabama, station. The dashed line shows the 95% confidence interval of the spread function of white noise variance. Diamonds show the variance as a function of the mean period for each IMF and the residual from the EMD decomposition of the annual mean temperature time series.

1. Estimate the slope of the residual of the empirical annually-averaged temperature record obtained by EMD decomposition with $\sigma_{thr}=0.3$.
2. Estimate the parameters of the null model from the monthly temperature station anomalies.
3. Generate ensembles of 1000 surrogate monthly temperature records, by taking into account the parameter uncertainties for each null model (Franzke, 2010, 2012).
4. Appropriately average the surrogate data so that they correspond to annual mean data.
5. Estimate the slopes of the surrogate data by EMD decomposition with $\sigma_{thr}=0.3$, i.e., in the same way as for the empirical data in step 1.
6. Compare the slope of the empirical trend with the distribution of surrogate slopes. If the empirical trend is outside the 2.5th or 97.5th percentiles of the surrogate distribution then we identify that this station has a trend that is unlikely to have arisen from the background climate variability described by the corresponding null model.

Here we use a standard approach to estimate the AR(1) parameters (Hosking, 1981; Franzke, 2010). The parameters of the FARIMA(0, d , 0) model, which is a particular case of the standard FARIMA(p , d , q) processes are estimated by a semi-parametric estimator (Geweke and Porter-Hudak, 1983; Hurvich and Deo, 1999) from detrended monthly temperature anomalies. Note

3.3 Results

that the surrogate data are generated on monthly time scales, which is less than the annual averaging period used for the empirical data. This is in order to include the effect of so-called climate noise, in which the averaging of rapid fluctuations produces variability on much longer time scales and apparent trends (*Leith, 1973; Feldstein, 2000; Franzke, 2009*).

3.3 Results

3.3.1 Statistical significance of linear slopes

The results of the Monte Carlo trend analysis described above is summarised in fig. 3.4 and table 3.1. As expected, stations with a linear slope close to zero were preferentially excluded by the null model tests, corresponding to a flat trend or an oscillating residual $r_m(t)$, as illustrated in fig. 3.5. (Compare with the significant trend shown in fig. 3.2.) Out of all 1167 stations, 900 (77%) have a significant trend against the white noise null model, 616 (52.8%) against the SRD model and 751 (64.5%) against the LRD model. Thus, interestingly, whilst all stations which are significant against the SRD model are also significant against the white noise model, the number of significant trends does not simply depend on the correlation range of the null model.

Null model	# of stations	% of dataset	Trend ($^{\circ}\text{C}/\text{century}$)
white noise	900	77.1	0.667 ± 0.711
SRD	616	52.8	0.876 ± 0.730
LRD	751	64.5	0.778 ± 0.713
all	593	50.8	0.898 ± 0.731

Table 3.1: Number and percentage of statistically significant annual mean temperature trends, and the spatially-averaged trend slope, as a function of the different null models.

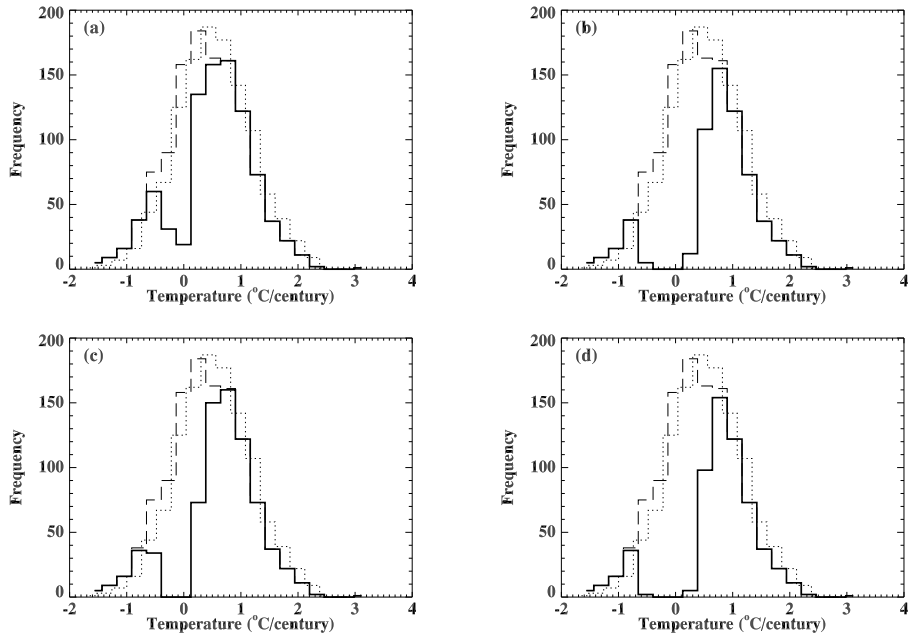


Figure 3.4: Distribution of annual mean temperature trend slopes for stations with a significant trend against: white noise (panel a), SRD (panel b), LRD (panel c) and all null models (panel d). Trend slopes for all stations from raw data (dotted line) and from EMD trend (dashed line).

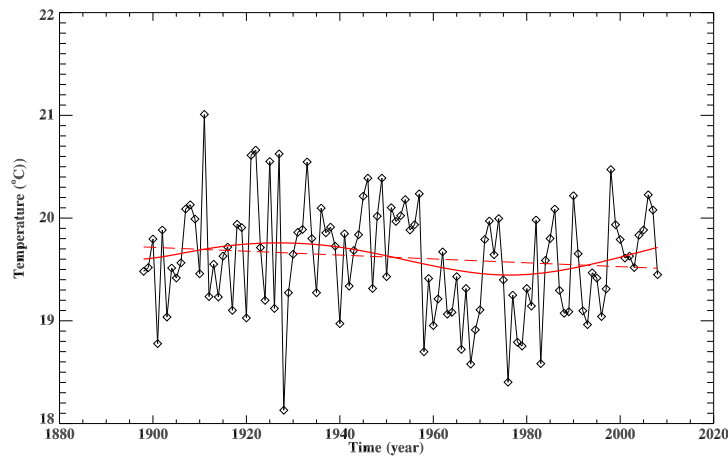


Figure 3.5: Annual mean temperature time series for Fairhope, Alabama, station. EMD trend is the solid red line and the dashed line is linear least square fit of the EMD trend.

3.3 Results

Overall, 593 stations (50.8% of all stations) show a significant trend against all three null models. This provides strong evidence (*Franzke, 2012*) for large-scale temperature change of the contiguous US over the last century, confirming and extending the results of previous studies (*Jones et al., 1999; Hansen et al., 2001; Lund et al., 2001; Lu et al., 2005*) which tested trends against only white noise or SRD models.

The average significant trend corresponds to an increase of temperature during the last century over the USA. However, the trend distributions display both significant cooling trends (negative slope) as well as significant warming trends (positive slope). These vary in location as shown in fig. 3.6 for significant EMD trends against all null models, and in fig. 3.7 for trends obtained by a linear least square of the raw station data. In figure 3.6 we show that both the widespread significant warming trends and the smaller region of significant cooling trends (in the south-east of the USA close to the southern Appalachian Mountains) reported by others (*Lu et al., 2005*) are robust to the correlation structure of the null model, including the LRD model not previously tested.

To gain insight into the likelihood of finding significant trends in a region we subdivided the US into grid cells of the same size (about 400 km²) and then computed the ratio of stations with significant trends against all three null models and the total number of stations in the grid cell. Figure 3.8 shows the geographic variation of this probability. There is a large region covering the South-East US and states like Pennsylvania and Ohio as well as regions in the North-West (parts of Washington State and Montana) which have a low probability of significant trends against all three null models, although note that these are generally greater than the assumed 5% critical probability. Furthermore, large parts of the contiguous US have probabilities of 50% or higher of significant trends against all three null models.

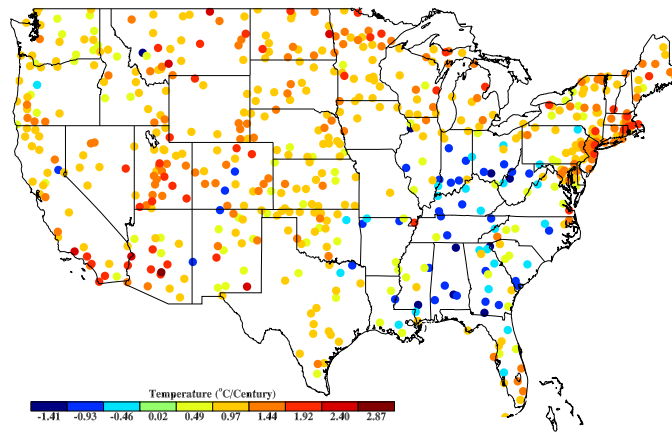


Figure 3.6: Geographical distribution of the slopes of the EMD annual mean temperature trend for the 593 stations with a significant trend against all null models.

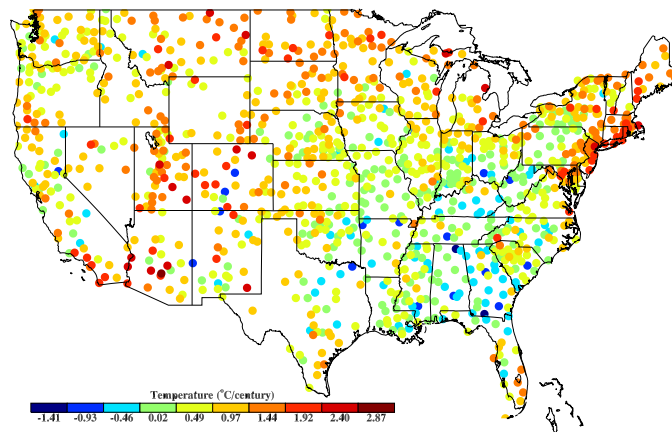


Figure 3.7: Geographical distribution of the slopes of the linear least-squares fit to the raw annual mean temperature data.

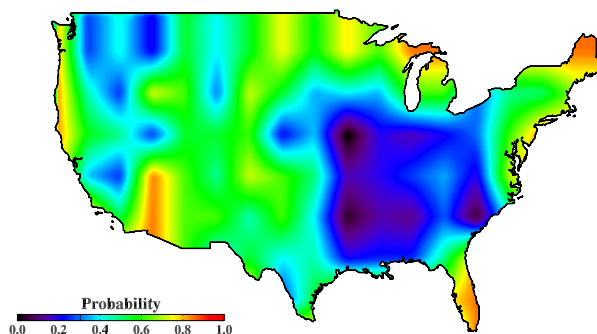


Figure 3.8: Geographical distribution of the probability to have a significant temperature trend against all three null models.

3.3.2 Nonlinear trend and local geographic parameters

The advantage of EMD is to obtain the residual as a time dependent nonlinear function without any a priori assumption about its structural form (see eq. 3.1). For each station at a given time t we have the trend slope and its derivative. This information allows us to investigate the climate trends from a point of view that is local in time. In figure 3.9 we show a map which displays the temporal evolution of the time derivative of the EMD trends. The derivative is obtained numerically through second order finite differences for each station. The stations are sorted according to the latitude (panel a) and longitude (panel b). Coherent structures are evident, suggesting robust relationships. As regard to the latitude we can see an increase of temperatures starting around 1920, but with a lag of about 30 years for the stations situated below of 35°N . For the longitude we can note a homogeneity in the onset time of warming, except for a middle strip from -90° to -80° where it is not possible to detect any positive (warming) trend, and including the region of significant cooling in the south-east US seen in fig. 3.7.

A similar plot was also made using altitude as a parameter (fig. 3.10). A positive trend seems to begin around 1920 at high and low altitudes and appears to descend and ascend respectively towards 800 – 900 m altitude in the following years.

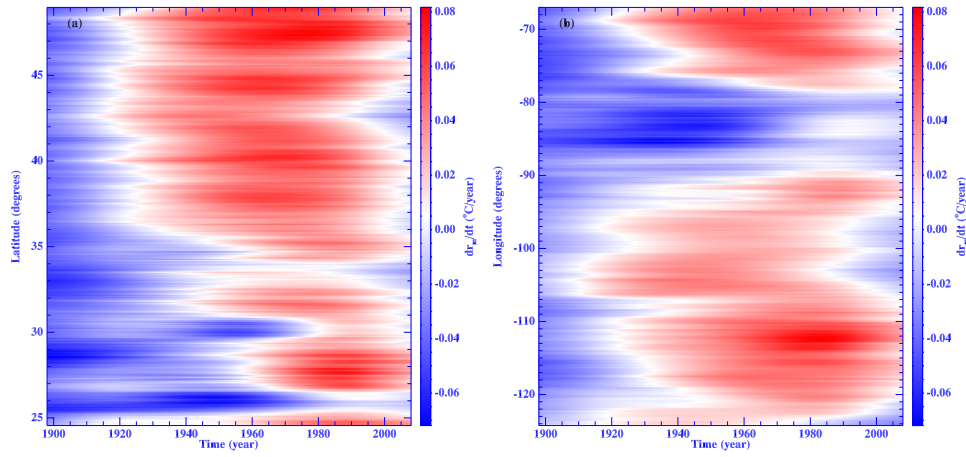


Figure 3.9: Contours of the derivative of EMD trends in a space-time plane for the 593 USA stations with a significant trend against all three null models. The y-axis represents the latitude (panel a) and longitude (panel b).

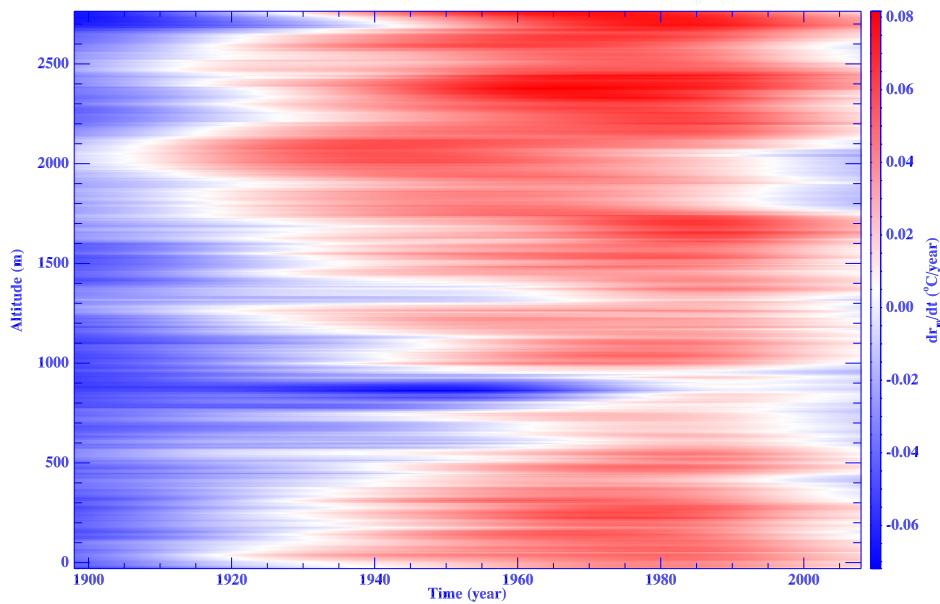


Figure 3.10: Contours of the derivative of EMD trends in a space-time plane for the 593 USA stations with a significant trend against all three null models. The y-axis represents the altitude.

3.4 Summary

In this study we discussed the spatio-temporal distribution of station temperature trends over the contiguous USA covering the period 1898 through 2008. We use the EMD decomposition to extract trends in a non-stationary situation (*Wu et al.*, 2007). Our main results can be summarized as follows:

1. We defined temperature trends as the residual of an EMD analysis. The most commonly used definition of a trend, which is a straight line fitted to the raw data, has been compared with the straight line fitting of the residual EMD function $r_m(t)$. The EMD analysis additionally reveals deviations from linear temperature trends. Our results extend the previous works about the temperature trends (*Jones et al.*, 1999; *Hansen et al.*, 2001; *Lund et al.*, 2001; *Lu et al.*, 2005) providing a more detailed view of the geographic distribution of the positive (warming) and negative (cooling) slopes.
2. By comparing these trends against three different null models for the background climate variability, we have increased confidence in the significance of the observed trends. About 50% of all stations are found to be significant against all three null models. This provides strong evidence that the US has experienced climate change over the last century, irrespective of the assumed correlation structure of the null model.
3. The region spanning the South-East US up to the states of Ohio and Illinois have seen a significant cooling trend while most other regions experienced a significant warming trend.
4. Using the time derivative of the residual EMD function $r_m(t)$, we can define the instantaneous changing slope of temperatures. We found that the changing slope is well ordered by the geographical longitude, latitude and altitude of the place where measurements are taken, and suggests that the onset of warming migrated in latitude and altitude.
5. Our results show that some care must be taken as far as detrending of climatic data records are concerned, as well as for the extrapolation of future climate change from trends.

Taken together, using an updated data set covering an extended period than previous studies (*Lund et al.*, 2001; *Lu et al.*, 2005), our results strengthen, support, and extend the evidence of a significant cooling in the South-East US and of a dominant significant warming over most of the contiguous US during the last century.

Chapter 4

Sun and oceans

In this chapter we report a study about two other complex phenomena related to climate: solar magnetic activity and ocean circulation and propagation.

The Earth receives almost all of its energy from the Sun, so the climate is strongly affected by solar power variation. Many scientists have observed correlations between the solar magnetic activity, which is reflected in the sunspot frequency, and climate parameters at the Earth. But sunspots are only the largest and by far the rarest of the broad range of magnetic features (magnetic flux tubes) in the solar photosphere. The smaller flux tubes forming the Bright Points and the network are bright. Like sunspots they also inhibit convection in their interiors, but they are sufficiently narrow that radiation flowing in from the sides into the highly evacuated flux tubes more than compensates for this loss. We studied pair dispersion of photospheric bright points to understand diffusion and transport of magnetic fields within the turbulent motions in the solar convection zone.

As the Sun also the oceans play a important role in climate influence the climate by transporting heat, with the atmosphere form the most dynamic component of the climate system. The ocean's waters are constantly being moved about by powerful currents that influence the climate by transporting heat. We investigated the oceanic propagation through the possibility that the tsunami, generated as a consequence of the large Tohoku-Oki earthquake of March 11th 2011, could be recorded by the tide gauge stations located in the Mediterranean sea.

4.1 Pair dispersion of photospheric bright points

Understanding the diffusion and transport of magnetic fields within the turbulent motions in the solar convection zone and atmosphere is of fundamental importance for several solar physics problems, such as dynamo, magnetoconvection, and energy release processes in the atmosphere. In this context,

the motions of local magnetic flux concentrations and magnetic bright points (BPs) represent one of the main sources of information.

These magnetic elements represent the photospheric signature of strong, *i.e.*, kilogauss, magnetic flux tubes and undergo random walk motions driven by turbulent convection. These motions have been studied extensively as a diffusion process and in this framework they have been investigated through the analysis of scaling properties of mean-square displacements $\langle(\Delta l)^2\rangle$ with time. For normal diffusion (in two dimensions), $\langle(\Delta l)^2\rangle = 4Kt$ where K is the diffusion coefficient. When $\langle(\Delta l)^2\rangle \sim t^\gamma$, with $\gamma \neq 1$, the diffusion is called anomalous. The cases $\gamma < 1$ and $\gamma > 1$ are called sub-diffusion and super-diffusion, respectively.

Previous studies of the diffusion properties of magnetic elements and photospheric G-band BPs have shown significant discrepancies. In some cases, normal diffusion has been reported, but with different values of the diffusion coefficient. In a recent paper, Abramenko et al. (Abramenko et al., 2011) used the very high resolution data on solar granulation obtained with the New Solar Telescope (NST; Goode et al. (Goode et al., 2010)) of the Big Bear Solar Observatory (BBSO) to study diffusion properties of BPs. They reported super-diffusion with $\gamma = 1.48$ in the AR plage area, $\gamma = 1.53$ in the quiet-Sun (QS) area, and $\gamma = 1.67$ in the coronal hole (CH).

The aim of this work is to study the pair dispersion of BPs by using the same NST observations as in Abramenko et al. (Abramenko et al., 2011), allowing us to access more direct information about turbulence properties of the solar photosphere

4.1.1 Observations, analysis and results

Solar granulation data were obtained with the NST of BBSO in 2010 August-September. Series of speckle-reconstructed images taken with a TiO filter (centered at a wavelength of 705.7 nm, with a bandpass of 1 nm) for three magnetic environments on the Sun were utilized. Namely, we analysed (1) the quiet-Sun internetwork/network area, (2) CH area and (3) plage area inside an AR.

Bright features, apparent inside dark inter-granule lanes, are called BPs and they are thought to be footpoints of magnetic flux tubes (Muller et al., 2000; Berger and Title, 2001; Ishikawa et al., 2007). Therefore, studying BPs makes it possible for us to measure the dynamics of the photospheric magnetic flux tubes. BPs were automatically detected in all images and then tracked from one image to the next. We used the detection and tracking code previously described in Abramenko et al. (Abramenko et al., 2010). BPs are first enhanced in the images and then selected by applying thresholding and masking. When two elements merged, the tracking of the smallest one was terminated.

A common approach used to study the dynamics of magnetic elements

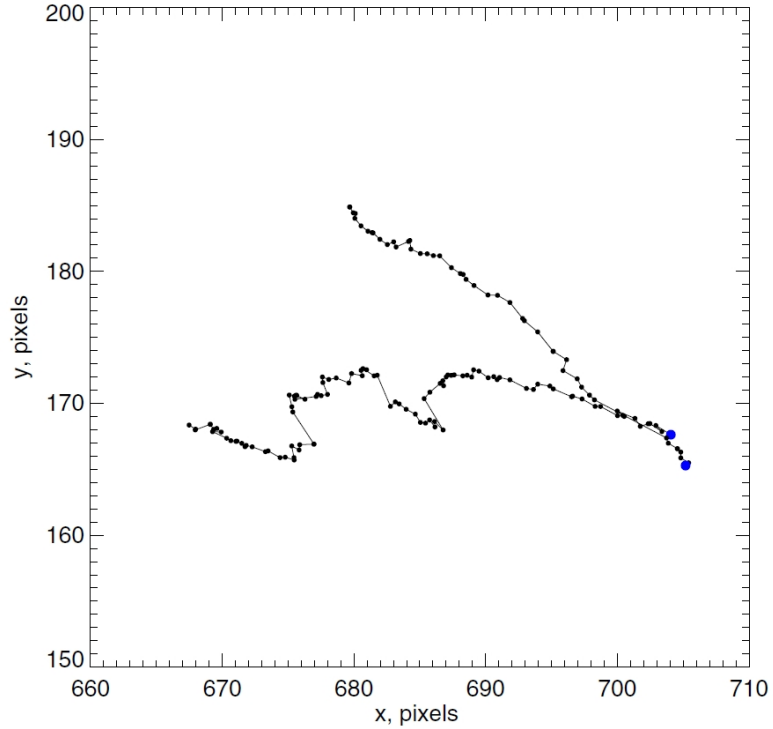


Figure 4.1: Trajectories of a pair of BPs separating from their initial positions, marked with the blue circles.

consists in considering the diffusion process of these elements as a result of the turbulent fluid motions occurring in the convection zone and in the photosphere. In other words, it is assumed that magnetic flux concentrations are transported by turbulent flows and that they can be treated as Lagrangian "fluid particle". Following this idea, we utilize here the Lagrangian approach to investigate the turbulent pair dispersion of BPs in the solar photosphere.

Our first step is to compute the pair separations $\mathbf{r}_{ij} = \mathbf{X}_i(t) - \mathbf{X}_j(t)$ of two BPs as a function of time interval, t , measured in seconds, where $\mathbf{X}_i(t) = (x_i(t), y_i(t))$ and $\mathbf{X}_j(t) = (x_j(t), y_j(t))$ are the coordinates of the i th and j th BPs at the time instant t . Figure 4.1 shows a typical example of a pair of BP trajectories separating with time. We then calculate the averages (over all pairs) $\Delta^2 = \langle [\mathbf{r}(t) - \mathbf{r}_0]^2 \rangle$ as a function of time, where \mathbf{r}_0 are the initial pair separations.

This procedure is repeated for the QS, CH, and ARP data in order to compare the pair dispersion properties in these different areas (Figure 4.2). A power law $\Delta^2(t) \sim t^\eta$ is found for the mean-squared separation in the range $10s < t < 400s$ with $\eta = 1.469 \pm 0.006$ for QS areas, $\eta = 1.469 \pm 0.009$ for CH areas, and $\eta = 1.487$ for ARP areas. This result can be compared with the analysis of the mean separation of randomly selected BP pairs performed

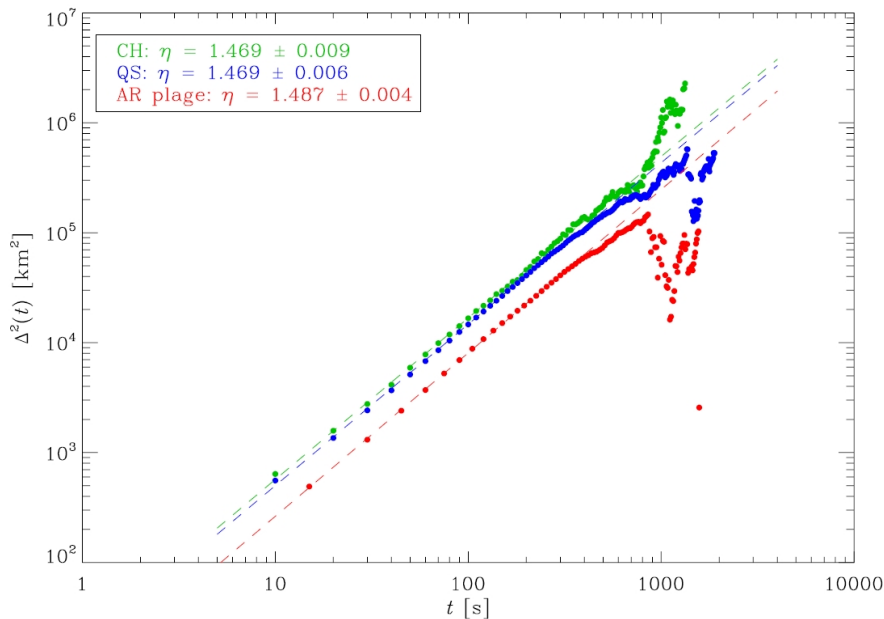


Figure 4.2: Mean-square BP separation $\Delta^2(t)$ determined for the CH data (green), QS area (blue), and AR plage area (red). The dashed lines represent power laws $\Delta^2(t) \sim t^\eta$, with the values of the power-law index η obtained from best fits in the range $10s < t < 400s$ and shown in the inset.

by Berger et al. (*Berger and Title, 2001*). For $t > 400s$ it can be seen that the statistics is not sufficient to identify breaks and other scalings, such as the Richardson law. The ARP data show the smallest BP separations as expected, since the BP surface density is larger in ARP areas compared to CH and QS (*Abramenko et al., 2011*).

This result is shown to be consistent with scaling laws of turbulent pair dispersion obtained in a non-asymptotic regime in which the Lagrangian tracers keep memory of their initial separations. Due to the lack of sufficient statistics of tracked BPs it is currently not possible with the observations at our disposal to know if the observed scaling extends also for $t > 400s$ or if other scaling regimes are present in the asymptotic range.

Further studies of BP pair dispersion can provide information about the magnetic field transport in the photosphere. Moreover, the transport properties of local magnetic field concentrations are closely related to the dynamics of solar atmosphere turbulence. The physical processes analysed in the present work represent one of the possible ways to investigate the efficiency of the turbulent energy transfer to small scales, which may play an important role in the energy dissipation processes occurring in the upper atmospheric layers.

4.2 Tsunami effects on Mediterranean

On March 11, 2011 at 05 : 46 : 23 UTC the NE coast of Honshu island (Japan) was struck by one of the largest earthquakes never occurred in the world since historical times. The Mw 9.0 event released accumulated tectonic stress over the last 700 years (*Inuma et al.*, 2011) and triggered a giant tsunami that caused an estimated losses of 200-300 billion US dollars and killed more than 10,000 people living along the coasts of Japan and elsewhere in the Pacific region (*Hayes*, 2011; *Hirose et al.*, 2011; *Inuma et al.*, 2011). The period of the tsunami waves ranges from few minutes to several tenths of minutes and generally it depends on the geographic location. At the same time, its amplitude is large enough to be identified within the normal tidal and non-tidal spectrum of sea-level variability processes (*Gill*, 1982; *Lambeck*, 1988; *Cartwright*, 1999). Recent studies showed that large tsunamis can propagate through the oceans even up to very distant regions (*Merrifield et al.*, 2005; *Titov et al.*, 2005; *Joseph et al.*, 2005; *Woodworth et al.*, 2005, 2010). Small amplitude sea level oscillations, superimposed to the normal tides, were recorded in connection with the eastern Indian ocean tsunami of December 26 2004, even along the coasts of the British Isles, at thousand of km away from the Mw 9.3 earthquake epicentre, even up the West coast of Africa. This results could explain the findings of an overall tendency of giant earthquakes to produce a global relative sea level variation (*Melini and Piersanti*, 2006).

The propagation of tsunami in oceans is a topic largely investigated by means of fluid numerical simulations in shallow water approximation (see e.g. (*Geist*, 2009; *Titov et al.*, 2005) and references therein). This approach allowed to understand many properties of the propagation, such as the role of the orientation and intensity of the offshore seismic line source and the trapping effect of mid-ocean ridge topographic wave guides that influences wave amplitude, directionality, and global propagation patterns (see e.g Ref. (*Titov et al.*, 2005)). On the other hand, the possibility that a tsunami wave, produced by a far seismic event, could affect in some way the Mediterranean sea, has received less attention. This is mainly attributable to the irregular bathymetry of the Gibraltar strait, that is believed to produce a strong damping and multiple reflections of the wave thus decreasing the probability of penetration in the Mediterranean basin. After the large 2004 Indian Ocean tsunami, additional improvements to global tide gauge systems were performed for the monitoring of both tsunamis (*Titov et al.*, 2005) and variations in sea level (*Woodworth et al.*, 2010). This allowed to achieve, also in the Mediterranean, real time data with a quite homogeneous spatial coverage and high time resolutions, needed to reveal possible low amplitude fluctuations due to the far field destabilizing effect of tsunamis in this basin.

4.2.1 Data analysis and results

We focused on 31 sea level data in the period 9-15 march 2011. The sea level signals, having a time sampling of 10 minutes and an accuracy of better than 1 cm, have been retrieved from the IOC sea level station monitoring¹, from the Institute for Environmental Protection and Research (ISPRA)² and from the Permanent Service for Mean Sea Level (PSMSL)³. The geographic distribution of the tide gauge stations is reported in fig.4.3. During the considered time window the weather situation around the stations was favourable (mainly calm sea, low and constant wind velocity), thus not inducing critical conditions of the sea surface for the quality of the sea level data set. Moreover, our analysis was restricted to the tidal stations located in sheltered positions; namely, the effects of both intensity and direction of the wind on the sea level recordings, based on the length of the fetch and the subsurface topography for the location, were negligible (*Gill, 1982*). Sea level observations were first reduced for atmospheric pressure variations by applying an inverse barometric correction to the data (*Wunsch and Stammer, 1997*).

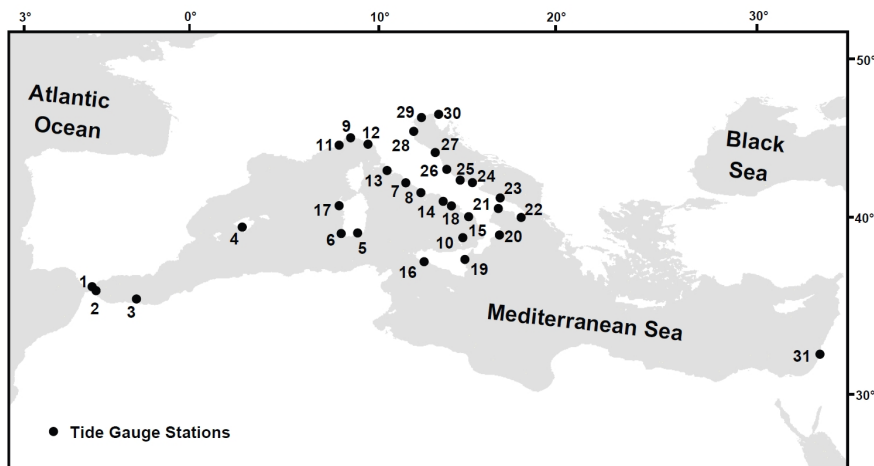


Figure 4.3: Map of the tide gauge stations, in the Mediterranean, used in this study. Numbers refer to the following stations: 1. Gibraltar, 2. Ceuta, 3. Melilla, 4. Palma de Mallorca, 5. Cagliari, 6. Carloforte, 7. Civitavecchia, 8. Gaeta, 9. Genova, 10. Ginostra, 11. Imperia, 12. La Spezia, 13. Livorno, 14. Napoli, 15. Palinuro, 16. Porto Empedocle, 17. Porto Torres, 18. Salerno, 19. Catania, 20. Crotone, 21. Taranto, 22. Otranto, 23. Bari, 24. Vieste, 25. Ortona, 26. San Benedetto, 27. Ancona, 28. Ravenna, 29. Venezia, 30. Trieste, 31. Hadera.

¹www.ioc-sealevelmonitoring.org

²www.mareografico.it

³www.pol.ac.uk

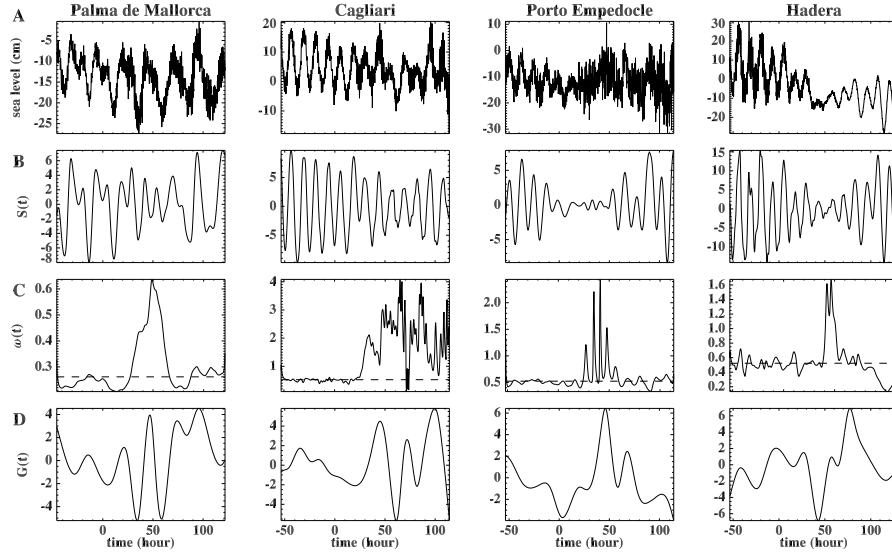


Figure 4.4: Time evolution of the sea levels (line A), contribution of the high amplitude components $S(t)$ (line B), instantaneous frequency of the highest amplitude IMF (line C), low frequency contribution $G(t)$ (line D) for the stations of Palma de Mallorca (4), Cagliari (5), Porto Empedocle (16) and Hadera (31). Time is counted from the origin time of the Tohoku-Oki earthquake. The dashed line corresponds to $(2\pi)/12$ hour $^{-1}$ for Cagliari, Porto Empedocle and Hadera and $(2\pi)/24$ hour $^{-1}$ for Palma.

As an example raw data, in fig. 4.4 (row A) we show the sea level time series $L(t)$ at four stations. Time is measured as the lag from the earthquake occurrence. A sudden change of regime can be identified in all the signals after the earthquake. In fact, the regular tidal oscillation is broken, more frequencies appear, and the time behaviour becomes more complex and highly nonstationary. This kind of dynamical behaviour is common to all the records we investigated. In fig. 4.5 we report the sea level time series $L(t)$ for the Cagliari station (panel a), along with the 12-hours return map $L(t + \Delta)$ vs. $L(t)$, for $\Delta = 12$ hours (panel b). The figure roughly provides evidences that after the main shock the Mediterranean sea felt a strong phase and amplitude perturbation of the tidal oscillation. In fact, for $t \leq 0$ (blue line), the points of the return map are approximately sorted along a straight line, indicating that the oscillation amplitude and phase remain almost constant. On the contrary for $t > 0$ (red line), the points are distributed on irregular ellipses, indicating that the phase and amplitude are no more constant but change with time.

In order to characterize the observed change of dynamical behaviour, we use the Empirical Mode Decomposition (EMD) (see appendix). Each sea level time series $L(t)$ is decomposed into a finite number n of Intrinsic Mode

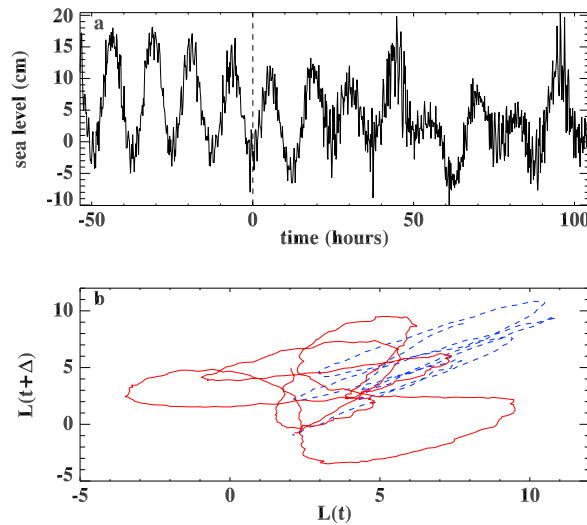


Figure 4.5: Time evolution of the sea level $L(t)$ (panel a) and the 12-hours return map $L(t + \Delta)$ vs. $L(t)$ (panel b) for the Cagliari station ($\Delta = 12$ hours). Time is counted from the origin time of the Tohoku-Oki earthquake. Blue dashed line refers to times $t \leq 0$, red full line refers to times $t > 0$.

Functions (IMF) $\theta_j(t)$ as

$$L(t) = \sum_{j=0}^{n-1} \theta_j(t) + r_n(t) . \quad (4.1)$$

The IMFs, containing information about the local properties of the signal are empirical, *i.e.* not given a priori but obtained from the data by following the "sifting" method (?). At the end of the procedure n empirical modes, ordered with increasing characteristic time scale, and a residue $r_n(t)$, which describes the mean trend if any, are obtained. The orthogonality of EMD decomposition ensures that each IMF captures the empirical dynamical behaviour of a single independent mode of the system, namely each j -mode describes a single phenomenon within the complex dynamics. This allows to filter and reconstruct the signal through partial sums in Equation (4.1) in order to obtain independent contributions to the signal in different ranges of time scales (*Huang et al.*, 1998; *Terradas et al.*, 2004; *Vecchio et al.*, 2010).

When applied to the Mediterranean tide gauge data the EMD gives a number n of modes which in general depends on the station under analysis. As obtained from the test of significance for the various IMFs (*Wu and Huang*, 2004), the first three modes, $j \leq 2$, represent high frequency noise while higher j modes are associated with significant oscillations of the sea level at different time scales. For the majority of the stations the IMF with the highest amplitude has a period of $\tau \approx 12$ hours, corresponding to the well known semidiurnal

oscillation. However, in the analysed data sets, the full semidiurnal component of the tide is split in two or three IMFs, depending on the station. This means that one IMF does not suffice to fully describe the temporal behaviour of the 12 hours tidal component. The previous result follows from the high sensitivity of the EMD to local frequency fluctuations. The latter, still persisting when meteorological effects have been removed, are strong enough as to affect the regularity of the semidiurnal mode of oscillation. As mentioned before, since for the properties of the EMD decomposition each IMF is associated to a well defined time scale of the signal at hand, a regular semidiurnal oscillation should be isolated in a single IMF. In presence of localized frequency fluctuations new time scales arise and affect the regular oscillation of the high energy tidal components. In this case, a single IMF is not able to account for the new timescales and the time evolution of the 12 hour oscillation is split in two or more IMFs. Of course, the sum of these EMD modes will describe the full contribution of the semidiurnal oscillation to the sea level. For Palma de Mallorca and the stations in the northern sector of the Adriatic sea (stations 26-30), the simultaneous presence of both diurnal and semidiurnal components, as main tidal constituents, has been detected. This is a well know phenomenon and it should depend, in the Adriatic sea, on the basin characteristics, i.e., the low sea depth and the semi-closed shape (*Janeković and Kuzmić, 2005; Capuano et al., 2011*). For these cases the previous considerations are also valid for the 24 hours component which is split in two IMF. By exploiting the orthogonality of the EMD decomposition, the signal $L(t)$ has been divided, by partial sum in equation (4.1), in four contributions namely $L(t) = \eta(t) + S(t) + G(t) + r_n(t)$. The function $\eta(t)$ is associated with the high-frequency noise, $S(t)$, obtained as the sum of of the high amplitude components (semi-diurnal and for some station also diurnal), represents the basic tidal mode and $G(t)$ describes the remaining low-frequency contribution. An example of the time behaviour of $S(t)$ is reported in row B of fig.4.4. Its dynamics is far from being regular and stationary since the waveforms abruptly change after $t = 0$. The variation of the main tidal contribution can be better appreciated by looking at the instantaneous frequency of the highest amplitude IMF (row C of fig. 4.4) which is abruptly destabilized in correspondence of the change of oscillating regime in $S(t)$ and departs from the constant value of $(2\pi)/12 \text{ hour}^{-1}$. Note that for Palma de Mallorca the reference frequency is $(2\pi)/24 \text{ hour}^{-1}$ since, in this case, the highest amplitude mode is associated with the diurnal component.

EMD modes with longer periods describe low-frequency phenomena. The function $G(t)$, an example is reported in row D of fig.4.4, is characterized by the increase of amplitude after $t = 0$. Figure 4.6 shows the contour plot of the functions $G(t)$, ordered according to the distance from Gibraltar. The figure clearly indicates that the time at which the increased amplitude regime is at its maximum absolute value is function of the distance from the Strait of Gibraltar. This result is consistent with a travelling perturbation in the

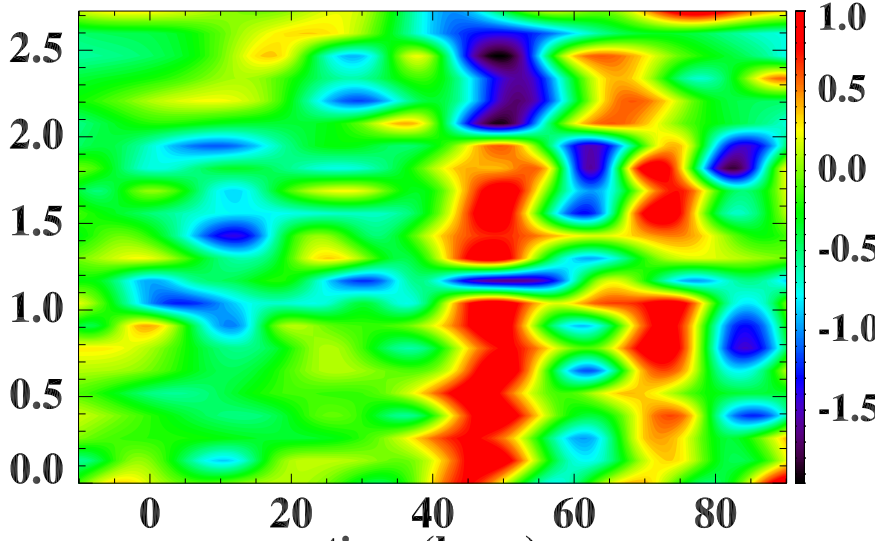


Figure 4.6: Contours of $G(t)$ in the space-time plane. The x -axis reports the time counted from the Tohoku-Oki earthquake, while the y -axis reports the distance in Km from Gibraltar.

whole Mediterranean sea propagating from Gibraltar. The Adriatic stations, for sake of clarity, have been excluded from fig.4.6. For these stations, due to the Adriatic basin geographic characteristics, the time-distance relation is inverted. In fact, the northernmost Adriatic stations are nearer to Gibraltar but the perturbation has to cover a longer path before reaching them. As shown in fig.4.6 the majority of stations shows a peak (in red) after $t = 0$, which indicates a positive fluctuation of the sea level. On the other hand, some records, including Hadera and the stations in the Ionian sea, are characterized by a drop (in blue) followed by the transient increase of the sea level. This behaviour can be induced by the local seafloor topography and/or to the different paths taken by the tsunami waves and reflection effects (*Joseph et al.*, 2005). The space-time representation allows to estimate the velocity of propagation of the perturbation, in the Mediterranean sea, as about $V_p \simeq 60$ m/s. Note that, this perturbation is revealed in the whole Mediterranean sea, being observed up to Hadera, the easternmost station, about 13 hours after Gibraltar.

We hypothesize that both the indirect perturbation on the tidal frequency and the direct transfer of small fluctuations beyond the Strait of Gibraltar, are generated from the tsunami triggered by the March 11th 2011, Tohoku-Oki earthquake. We remark that the timing of both these effects, varying between ~ 45 hours in Gibraltar and ~ 58 hours in Hadera, are in agreement with the results of theoretical models of tsunami propagation for which the perturbation should arrive at Gibraltar in a time of about 38 hours after the

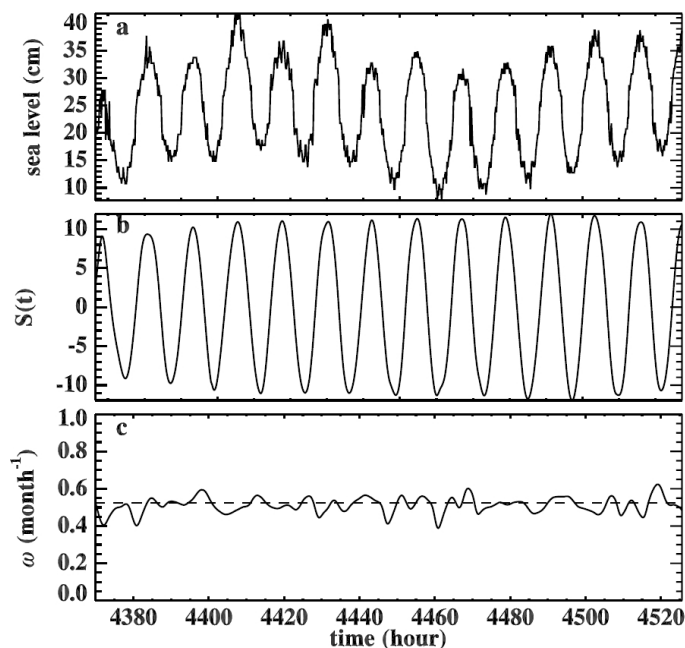


Figure 4.7: Time evolution of the sea levels (a), semidiurnal IMF (b) and instantaneous frequency (c) for the Cagliari station. Time is counted from the origin time of the Tohoku-Oki earthquake.

earthquake⁴. The obtained results have been tested by looking at the sea level records during the period 9-15 September 2011, in a time window which cannot be related with the Tohoku-Oki earthquake. We assume that, in this period, the possible transient effect of the tsunami is null and the system behaves according with the usual dynamics. As expected, we found that the principal tidal components shows a regular behaviour and are detected in a single IMF by the EMD. This indicates that the splitting of the principal tidal component in more IMFs along with the instantaneous frequency destabilization could be plausibly associated with a transient effects, associated with the tsunami. As an example, the results for the Cagliari station are reported in fig. 4.7. The raw data are shown in panel a), and panel b) shows the regular semidiurnal component associated with the largest amplitude IMF, whose characteristic time scale is 12.27 hours. Panel c) shows the instantaneous frequency of the IMF reported in panel b). The striking difference with Fig. 4.4 is evident. As expected, the frequency is centered around the value $2\pi/12 \text{ hour}^{-1}$ with low amplitude stochastic fluctuations superimposed.

⁴<http://nctr.pmel.noaa.gov/honshu20110311/honshu2011-globalmaxplot.png>

4.2.2 Summary

In this paper we investigated the anomalous sea level changes for 31 stations in the Mediterranean basin, due to a transient perturbation in the period 9 – 15 March 2011. Once the atmospheric pressure effects have been removed and the wind intensity and direction have been accounted for, with respect to the position of the individual tidal stations, we hypothesize that the perturbation is a consequence of the tsunami generated by the March 11th, 2011, Mw 9.0 Tohoku-Oki earthquake. Our analysis shows that the Mediterranean felt the effect of the tsunami 40 – 50 hours after the main shock thus indicating that tsunamis generated by strong earthquakes are truly global events. In particular, we revealed two kind of transient signatures. Firstly, the perturbation generates strong frequency fluctuations affecting the regular behaviour of the high amplitude tidal components, usually the semidiurnal and in some cases also the diurnal one. As a consequence of the perturbation, these components appear highly nonstationary and several IMFs are needed to reproduce their full contribution. In addition the instantaneous frequency shows abrupt destabilization after the earthquake occurrence. The physical mechanism causing these manifestations should be related to a resonant response to the tsunami at the strait entrance. Tides in enclosed basins, connected to the open sea by a narrow strait, can manifest amplified or damped response to a forcing action outside the basin (*Maas, 1997*). Due to nonlinear effects the basin may exhibit chaotic modulation of the tidal amplitude and frequency. Since the Mediterranean sea is similar to a closed basin with respect to the oceans and is connected to Atlantic Ocean by a narrow strait, it could be affected by the forcing action of the fluctuations associated with the tsunami and could manifest nonlinear response leading to amplification and frequency destabilization. The second signature consists in a propagating perturbation manifesting with a weak increase of amplitude of the low frequency EMD modes, after the occurrence of the Tohoku-Oki earthquake. This perturbation, significant with respect to the noise level, should be an evidence of the direct transmission of tsunami fluctuations, characterized by long periods, through the Gibraltar strait. The timing of the detected tidal perturbations at the recording stations are in agreement with the prediction of the global models of tsunami propagation, for which the arrival at the straits of Gibraltar is expected about 38 hours after the onset of the earthquake. Effects on sea levels due to post-seismic deformations (*Melini and Piersanti, 2006*), capable to cause global sea level raise of the order of a fraction of mm (<http://cires.colorado.edu/~bilham/Honshu2011/Honshu2011.html>) and direct propagation of surface seismic waves from the epicenter, arriving at the Mediterranean region 20 – 30 minutes after the mainshock (www.emsc-csem.org), have been excluded since not consistent with the observed sea level variations. Additionally, it is unlikely that free oscillations of the Earth, excited by the high magnitude Tohoku-Oki earthquake, originated the detected fluctuations since the timing and period

4.2 Tsunami effects on Mediterranean

INGV Istituto Nazionale di Geofisica e Vulcanologia

HOME | CHI SIAMO | SERVIZI | INCHIESTE | NOTIZIARI | COMUNICAZIONE E RELAZIONE | STAMPA | AREA RISERVATA

Sei in: [URLO stampa](#) > [STAMPA e COMUNICAZIONE](#) > [Attività Comunicati Stampa](#) > [Comunicati Stampa 2011](#) > [L'oscillazione nel Mar Mediterraneo dopo lo tsunami del marzo 2011 di Tohoku-Oki, isola di Honshu \(Giappone\)](#)

ENGLISH | CERCA

Comunicati Stampa
Rassegna Stampa
Newsletter
Archivio Rassegna Stampa dal 1980 al 2011
Archivio Interviste Radio e Televisione dal 2007 al 2011
Archivio Filmati INGV
Flickr

free rumble

L'oscillazione nel Mar Mediterraneo dopo lo tsunami del marzo 2011 di Tohoku-Oki, isola di Honshu (Giappone).

14/06/2012

L'11 marzo del 2011, una scossa sismica di magnitudo 9, colpì l'isola di Honshu, in Giappone, con il settimo sisma più potente nella storia dei terremoti conosciuti. Dal movimento tellurico, ne conseguì un'onda di tsunami che si propagò in gran parte degli Oceani. Oggi sappiamo che la perturbazione marina riuscì anche a passare attraverso lo Stretto di Gibilterra, causando deboli oscillazioni del Mare Nostrum. Queste sono state individuate grazie all'analisi di dati mareografici effettuata da un gruppo di studiosi dell'Istituto Nazionale di Geofisica e Vulcanologia - INGV, del Dipartimento di Fisica dell'Università della Calabria e del British Antarctic Survey, Natural Environment Research Council, Cambridge, UK (Antonio Vecchio, Marco Anzidei, Vincenzo Capparelli, Vincenzo Galone e Grazia Guarnì), che hanno pubblicato i loro risultati in un articolo scientifico dal titolo "Has the Mediterranean Sea felt the March 11th, 2011, Mw 9.0 Tohoku-Oki earthquake?" sulla prestigiosa rivista "EPL: A Letters Journal Exploring the Frontiers of Physics" (www.epjjournal.org).

Chiediamo a Marco Anzidei, ricercatore dell'INGV e uno dei coautori dello studio, come si è riuscito a ottenere questo risultato. Abbiamo analizzato i dati mareografici della rete italiana dell'ISPRA, anche grazie alla disponibilità dell'Ing. Giovanni Arena, e quelli delle stazioni internazionali afferenti al Permanent Service for Mean Sea Level. I dati sono stati analizzati con tecniche sofisticate e innovative che hanno permesso di individuare all'interno delle registrazioni il segnale legato agli effetti del maremoto del Giappone. L'oscillazione della superficie marina è arrivata nel Mediterraneo 40-50 ore dopo l'evento sismico.

L'innalzamento potrebbe mettere a rischio le coste italiane?

No, perché si è trattato di un fenomeno transiente e di piccola ampiezza, dell'ordine di 10-15 cm.

Studi recenti ipotizzano innalzamenti locali del mare Mediterraneo anche fino a 1.5 m entro fine secolo per cause climatiche e tettoniche. Quanto lo tsunami giapponese influenza questo dato?

È possibile che si sia verificata una variazione globale del livello del mare in seguito a questo maremoto, tuttavia non esistono ancora studi specifici come avvenuto ad es. per il maremoto di Sumatra del 2004. Ad ogni modo, l'ampiezza della variazione globale sarebbe molto piccola, dell'ordine del millimetro o meno.

Per l'approfondimento clicca qui: <http://www.freeumble.com/audio.php?audioId=3547>

Ufficio stampa@ingv.it 06.51980543-515

Figure 4.8: Press release of INGV.

of the main mode of oscillation (*Aki and Richards, 2002; Kanamori and Anderson, 1975*) are not in agreement with the timing and frequency of sea level perturbations revealed by our observations. However, based on the available seismological and geophysical literature (*Aki and Richards, 2002*) the effects of free oscillations of the Earth on the sea level have not yet investigated and the results presented in this paper provide new observational constraints for these studies. The physical mechanisms briefly described above, need deeper investigations and will be faced in a future paper.

This work, published on *EPL A Letters Journal Exploring the Frontiers of Physics* (*Vecchio et al., 2012*), after a press release of INGV (figure has been very successful and relief of many newspapers nations:

- *CORRIERE DELLA SERA link*
- *L'UNITÀ link*
- *ITALIA OGGI link*
- *ANSA link*
- *VIRGILIO NOTIZIE link*
- *TM NEWS link*
- *AGENZIA GIORNALISTICA ITALIANA link*
- *IL QUOTIDIANO DELLA CALABRIA link*
- *SUDMAGAZINE link*
- *24 ORE NOTIZIE link*
- *6 APRILE link*
- *FREE RUMBLE link*
- *INFOSANNIO link*

- WALL STRET ITALIA *link*
- METEO CAPRINO VERONESE *link*
- NEXT TIME *link*
- SILVER BACK *link*
- IN TOPIC *link*
- MEDITERRANEA NEWS *link*
- TRADING ON LINE *link*
- IL MONDO *link*
- AMBIENTE ECO SEVEN *link*
- ECOLOGIAE *link*

Appendix A

Empirical Mode Decomposition

The Empirical Mode Decomposition (EMD) is a new method for analysing nonlinear and non-stationary data and successfully applied in many different fields (*Loh et al.*, 2001; *Echeverria et al.*, 2001; *Coughlin et al.*, 2004; *Vecchio et al.*, 2010; *Laurenza et al.*, 2012; *Capparelli et al.*, 2011). Introduced by Huang et al. (*Huang et al.*, 1998) it decomposes the variance of signal into a finite number of intrinsic mode functions (IMFs) and a residue by using an adaptive basis derived from each data set through a so-called "sifting" process. Namely:

$$x(t) = \sum_{j=0}^{m-1} \theta_j(t) + r_m(t). \quad (4.2)$$

where $x(t)$ is a generic signal and each IMF $\theta_j(t)$ and residual $r_m(t)$ are time-dependent. The "sifting" algorithm works as follows:

1. all local maxima and minima of the time series $x(t)$ were identified
2. all local minima (maxima) were connected through a cubic spline as a lower (upper) envelope of the time series
3. the signal $h_1(t)$ was calculated as the difference between the raw data and the mean of lower and upper envelopes $m_1(t)$, namely $h_1(t) = x(t) - m_1(t)$
4. $h_1(t)$ is a first IMF only if it satisfies two criteria: (i) the number of extrema and the number of zero-crossing must either be equal or differ at most by one; (ii) at any point the mean value of the lower and upper envelope is zero. If $h_1(t)$ does not satisfy one of this terms, the step 3 is repeated using $h_1(t)$ as a raw data, namely, $h_{11}(t) = h_1(t) - m_{11}(t)$, where $m_{11}(t)$ is a mean of the envelopes derived from h_1 . This procedure is iterated k times until h_{1k} satisfies the conditions (i) and (ii).

To guarantee that the IMF components contain enough physical properties with respect to both amplitude and frequency modulations, a criterion to

stop the sifting process has been introduced (*Huang et al.*, 1998). Usually as stopping criterion the Cauchy-type convergence criterion has been used, where the sifting is carried to the point when the difference between the successive sifted results is smaller than a given limit (*Huang et al.*, 1998). By introducing a kind of standard deviation σ defined as:

$$\sigma = \sum_{t=0}^N \left[\frac{|h_{1(k)}(t)| - |h_{1(k-1)}(t)|}{h_{1(k-1)}^2(t)} \right] \quad (4.3)$$

the "sifting" process is stopped when σ is smaller than a threshold value σ_{thr} , which generally is fixed as $\sigma_{thr}=0.3$. By construction, the number of extrema is decreased when going from one residual to the next (thus guaranteeing that the complete decomposition is achieved in a finite number of steps), and the corresponding spectral supports are expected to decrease accordingly. While modes and residuals can intuitively be given a "spectral" interpretation, it is worth stressing the fact that, in the general case, their high vs. low frequency discrimination applies only locally and corresponds by no way to a pre-determined sub band filtering (as, *e.g.*, in a wavelet transform). Selection of modes rather corresponds to an automatic and adaptive (signal-dependent) time-variant filtering.

Each IMF has its own timescale, τ_j , and represents a zero mean oscillation experiencing amplitude and frequency modulations; namely the j -th IMF can be written as $\theta_j(t) = A_j(t) \cos[\omega_j(t) \cdot t + \varphi_j]$, where $A_j(t)$ and $\omega_j(t)$ are the time dependent amplitude and frequency of the j -th mode, respectively. The IMF timescale is computed as the average time between local maxima and minima. The EMD allows to define, for each IMF, a meaningful instantaneous frequency calculated as follows. The Hilbert transform is applied on each IMFs, namely

$$\theta_j^*(t) = \frac{1}{\pi} P \int_{-\infty}^{\infty} \frac{\theta_j(t')}{t-t'} dt' \quad (4.4)$$

where P indicates the Cauchy principal value. $\theta_j(t)$ and $\theta_j^*(t)$ form the complex conjugate pair so that the instantaneous phase can be calculated as $\phi_j(t) = \arctan[\theta_j^*(t)/\theta_j(t)]$. The instantaneous frequency follows as $\omega_j(t) = d\phi_j/dt$. This definition of $\omega(t)$ is quite general and in principle some limitations on the data are necessary in order to obtain instantaneous frequency as single value function of time. The latter property is fulfilled by the EMD basis functions which allow to obtain meaningful instantaneous frequency consistent with the physics of the system under study (*Huang et al.*, 1998).

The EMD represents a powerful tool for time-frequency analysis of non-linear and nonstationary data. Being based on an adaptive basis, it allows to overcome some disadvantages of the Fourier spectral analysis when applied to real nonperiodic and nonstationary data, such as the a priori definition of the Fourier modes, that often are far from being proper eigenfunctions of the phenomenon at hand. Moreover, when dealing with nonperiodic data, Fourier

modes are mixed together in order to build up a solution corresponding to the fictitious periodic boundary conditions imposed by the analysis. On the other hand, the EMD does not introduce spurious harmonics, as in case of Fourier analysis, in reproducing non-stationary data and nonlinear waveform deformations. The EMD frequency is derived by differentiation rather than convolution, as in case of Fourier, and, therefore, there is not an uncertainty principle limitation on time or frequency resolution. With the above definition of $\omega(t)$ both inter- and intra-wave frequency modulations, due to waveform deformation by nonlinear effects and the dispersive propagation of waves respectively, can be detected. Note that the possibility to describe frequency modulations is completely lost in Fourier analysis, and only the interwave frequency modulation can be roughly recognized through the wavelet analysis (*Huang et al.*, 1998). We remark that τ_j cannot be interpreted as the period of Fourier modes since it provides just an estimate of the timescale characterizing the IMF for which it is computed. The EMD decomposition is complete and orthogonal (*Huang et al.*, 1998; *Cummings et al.*, 2004). The latter property, even if not theoretically guaranteed, is practically fulfilled (*Huang et al.*, 1998) and should be checked numerically *a posteriori*.

Bibliography

- Abramenko, V., V. Yurchyshyn, P. Goode, and A. Kilcik (2010). Statistical distribution of size and lifetime of bright points observed with the new solar telescope. *Astrophys. J.*, 725, L101. 58
- Abramenko, V. I., V. Carbone, V. Yurchyshyn, P. R. Goode, R. F. Stein, F. Lepreti, V. Capparelli, and A. Vecchio (2011). Turbulent diffusion in the photosphere as derived from photospheric bright point motion. *Astrophys. J.*, 743, 133. 58, 60
- Aki, K., and P.G. Richards (2002). Quantitative Seismology, 2nd Edition. University Science Books, Herndon, (USA). 69
- Alley, R. B., J. Marotzke, W. D. Nordhaus, J. T. Overpeck, D. M. Peteet, R. A. Pielke, R. T. Pierrehumbert, P. B. Rhines, T. F. Stocker, L. D. Talley, and J. M. Wallace (2003). Abrupt Climate Change. *Science*, 299, 2005–2010. 9, 10
- Arnold, V. I. (1965). Small denominators. I. mappings of the circumference onto itself. *AMS Trans. Series 2*, 46, 213–284. 18, 20
- Barbosa, S. M. (2011). Testing for Deterministic Trends in Global Sea Surface Temperature. *J. clim.*, 24, 2516–2522. 44
- Bar-Yam, Y. (1997). *Dynamics of Complex Systems*, Westview Press, 864 pp. 3, 4
- Berger, T. E., and A. M. Title (2001). On the Relation of G-Band Bright Points to the Photospheric Magnetic Field. *Astrophys. J.*, 553, 449–469. 58, 60
- Bunde, A., J.F. Eichner, S. Havlin, E. Koscielny-Bunde, H.-J. Schellnhuber and D. Vyushin (2004). Comment on "Scaling of Atmosphere and Ocean Temperature Correlations in Observations and Climate Models. *Phys. Rev. Lett.*, 92, 039801. 27, 34
- Capparelli, V., A. Vecchio, and V. Carbone, (2011), Long-range persistence of temperature records induced by long-term climatic phenomena, *Phys. Rev. E*, 84, 46103–46111. 46, 71

- Capuano, P., E. De Lauro, S. De Martino, and M. Falanga (2011). Water-level oscillations in the Adriatic Sea as coherent self-oscillations inferred by independent component analysis. *Progress in Oceanography*, 91, 447–460. 65
- Cartwright, D.E. (1999). Tides, A Scientific History. Cambridge University Press, Cambridge (UK). 61
- Charney, J. G., and J. Devore (1979). Multiple flow equilibria in the atmosphere and blocking. *J. Atmos. Sci.*, 36, 1205. 26
- Cook, E. R., D. M. Meko, and C. W. Stockton. A New Assessment of Possible Solar and Lunar Forcing of the Bidecadal Drought Rhythm in the Western United States.. *J. clim.*, 10, 1343–1356. 18, 23
- Cook, E., D. Rosanne, J. Cole, D. Stable, and R. Villalba (2000). Tree-ring records of past ENSO variability and forcing, in El Niño and the Southern Oscillation: Multiscale Variability and Global and Regional Impacts, Cambridge Univ. Press, 2000. 10
- Coughlin, K. T., and K. K. Tung (2004), 11-Year solar cycle in the stratosphere extracted by the empirical mode decomposition method, *Adv. Space. Res.*, 34, 323–329. 46, 71
- Croisier, H., M. R. Guevara, and P. C. Dauby (2009). Bifurcation analysis of a periodically forced relaxation oscillator: Differential model versus phase-resetting map. *Phys. Rev. E*, 79, 016209–016229. 18
- Cummings, D. A. T., R. A. Irizarry, N. E. Huang, T. P. Endy, A. Nisalak, K. Ungchusak, and D. S. Burke (2004). Travelling waves in the occurrence of dengue haemorrhagic fever in Thailand. *Nature*, 427, 344–347. 73
- Currie, R. G. (1984). Evidence for 18.6-year lunar nodal drought in Western North America during the past millennium. *Journal of Geophysical Research (Oceans)*, 89, 1295–1308. 23
- Ditlevsen, P. D. , H. Svensmark, and S. Johnsen (1996). Contrasting atmospheric and climate dynamics of the last-glacial and Holocene periods. *Nature*, 379, 810. 26
- Echeverria, J. C., J. A. Crowe, M. S. Woolfson, and B. R. Hayes-Gill (2001), Application of empirical mode decomposition to heart rate variability analysis, *Med. Biol. Eng. Comput.*, 39, 471–479. 46, 71
- Efstathiou, M.N., and C.A. Varotsos (2010). On the altitude dependence of the temperature scaling behaviour at the global troposphere. *International Journal of Remote Sensing*, 31, 343–349. 27

BIBLIOGRAPHY

- Eichner, J.F., E. Koscielny-Bunde, A. Bunde, S. Havlin, and H.-J. Schellnhuber (2003). Power-law persistence and trends in the atmosphere: A detailed study of long temperature records. *Phys. Rev. E*, 68, 046133. 26, 27
- Fatichi, S., S. M. Barbosa, E. Caporali, and M. E. Silva (2009). Deterministic versus stochastic trends: Detection and challenges. *J. Geophys. Res.*, 114, D18121. 44
- Feldstein, S. B. (2000). The Timescale, Power Spectra, and Climate Noise Properties of Teleconnection Patterns. *J. Climate*, 13, 4430–4440. 49
- Fraedrich, K., and R. Blender (2003). Scaling of Atmosphere and Ocean Temperature Correlations in Observations and Climate Models. *Phys. Rev. Lett.*, 90, 108501. 26, 27, 35, 40
- Fraedrich, K., U. Luksch and R. Blender (2004). Scaling of Atmosphere and Ocean Temperature Correlations in Observations and Climate Models. *Phys. Rev. E*, 70, 037301 (2004). 26
- Fraedrich, K., and R. Blender (2004). Fraedrich and Blender Reply. *Phys. Rev. Lett.*, 92, 039802. 27, 34, 35
- Franzke, C. (2009), Multi-Scale Analysis of Teleconnection Indices: Climate Noise and Nonlinear Trend Analysis, *Nonlin. Proc. Geophys.*, 16, 65–76. 44, 49
- Franzke, C. (2010), Long-Range Dependence and Climate Noise Characteristics of Antarctic Temperature Data, *J. Climate*, 23, 6074–6081. 44, 45, 48
- Franzke, C. (2012), Nonlinear trends, long-range dependence and climate noise properties of surface air temperature, *J. Climate*, 25, 4172–4183. 44, 48, 51
- Franzke, C., T. Graves, N. W. Watkins, R. Gramacy and C. Hughes (2012). Robustness of estimators of long-range dependence and self-similarity under non-Gaussianity. *Phil. Trans. Roy. Soc. A.*, 370, 1250-1267. 47
- Geist, E.L. (2009). Local tsunamis and earthquake source parameters. *Advances in Geophysics*, 51, 107–169. 61
- Geweke, J., and S. Porter-Hudak (1983). The estimation and application of long-memory time series models. *J. Time Ser. Anal.*, 4, 221–238. 48
- Gill, A. E. (1982). *Atmosphere-Ocean Dynamics*. Academic Press, New York (USA). 61, 62
- Glass, L., and M. C. Mackey (1979). A simple model for phase locking of biological oscillators. *Journal of Mathematical Biology*, 7, 339–352. 18

-
- Glass, L. (2001). Synchronization and rhythmic processes in physiology. *Nature*, *410*, 277–284. 18
- Goode, P.R., R. Coulter, N. Gorceix, V. Yurchyshyn, and W. Cao (2010). The NST: First results and some lessons for ATST and EST. *Astron. Nachr.*, *331*, 620–623. 58
- Govindan, R.B., D. Vyushin, A. Bunde, S. Brenner, S. Havlin, and H.-J. Schellnhuber (2002). Global climate models violate scaling of the observed atmospheric variability. *Phys. Rev. Lett.*, *89* 028501. 26, 27
- Halpert, M. S., and C. F. Ropelewski (1992). Surface temperature patterns associated with the Southern Oscillation. *J. Climate*, *5*, 577–593. 38, 39, 41
- Hansen, J., R. Ruedy, M. Sato, M. Imhoff, W. Lawrence, D. Easterling, T. Peterson, and T. Karl (2001). A closer look at United States and global surface temperature change. *J. Geophys. Res.*, *106*, 23947–23964. 51, 55
- Hansen, J. E., and M. Sato (2005). Paleoclimate Implications for Human-Made Climate Change. *Climate Change*, 21–47. 6
- Hasselmann, K. (1997). Climate Change: Are We Seeing Global Warming?. *Science*, *276*, 914–915. 10
- Hawkins, E., and R. Sutton (2009), The potential to narrow uncertainty in regional climate predictions, *Bull. Amer. Met. Soc.*, *8*, 1095–1107. 44
- Hayes, G.P. (2011). Rapid source characterization of the 2011 Mw 9.0 off the Pacific coast of Tohoku Earthquake. *Earth Planets Space*, *63*, 529. 61
- Hirose, F., K. Miyaoka, N. Hayashimoto, T. Yamazaki, and M. Nakamura (2011). Outline of the 2011 off the Pacific coast of Tohoku Earthquake (M 9.0): Seismicity: foreshocks, mainshock, aftershocks, and induced activity. *Earth Planets Space*, *63*, 513–518. 61
- Hosking, J. R. M., (1981). Fractional differencing. *Biometrika*, *68*, 165–176. 47, 48
- Houghton, J. T. (1995). *Climate Change 1995: The Science of Climate Change*. Cambridge University Press, Cambridge, UK. 27
- Huang, N. E., et al. (1998), The empirical mode decomposition and the Hilbert spectrum for nonlinear and non-stationary time series analysis, *Proc. R. Soc. Lond. A*, *454*, 903–995. 12, 30, 45, 64, 71, 72, 73
- Hurrell, J.W., Y. Kushnir, G. Ottersen, and M. Visbeck (2010). An overview of the North Atlantic Oscillation: an overview. *Geophysical Monograph*, *134*, 1. 39

BIBLIOGRAPHY

- Hurvich, C. M., and R. S. Deo (1999). Plug-in selection of the number of frequencies in regression estimates of the memory parameter of a long-memory time series. *J. Time Ser. Anal.*, 20, 331–341. 48
- Huybers, P., and W. Curry (2006). Links between annual, Milankovitch and continuum temperature variability *Nature*, 441, 329–332. 9, 10, 45
- Iinuma, T., M. Ohzono, Y. Ohta, and S. Miura (2011). Coseismic slip distribution of the 2011 off the Pacific coast of Tohoku Earthquake (M 9.0) estimated based on GPS data—Was the asperity in Miyagi-oki ruptured?. *Earth Planets Space*, 63, 627. 61
- Imbrie, J., and Imbrie, J. Z. (1980). Modeling the climatic response to orbital variations. *Science*, 207, 943–953. 16
- Intergovernmental Panel on Climate Change: Third Assessment Report of the Intergovernmental Panel on Climate Change (2001), Cambridge Univ Press, Cambridge, UK. 43
- Ishikawa, R., S. Tsuneta, Y. Kitakoshi, Y. Katsukawa, J. A. Bonet, S. Vargas Dominguez, L. H. M. Rouppe van der Voort, Y. Sakamoto, and T. Ebisuzaki (2007). Relationships between magnetic foot points and G-band bright structures. *A&A*, 472, 911. 58
- Janeković, I., and M. Kuzmić (2005). Numerical simulation of the Adriatic Sea principal tidal constituents. *Ann. Geophys.*, 23, 1. 65
- Jiang, N., J. D. Neelin, and M. Ghil (1995). Quasi-quadrennial and quasi-biennial variability in the equatorial Pacific. *Climate Dynamics*, 12, 101–112. 10
- Jin, F., J. D. Neelin, and M. Ghil (1994). El Nino on the Devil’s Staircase: Annual Subharmonic Steps to Chaos. *Science*, 264, 70–72. 10
- Jones, P. D., M. New, D. E. Parker, S. Martin, and I. G. Rigor (1999). Surface air temperature and its changes over the past 150 years. *Rev. Geophys.*, 37, 173–199. 51, 55
- Jones, P. D., K. R. Briffa, and T. J. Osborn (2003). Changes in the Northern Hemisphere annual cycle: Implications for paleoclimatology?. *J. Geophys. Res.*, 108, 4588–4594. 10, 21
- Jones, P. D., D. H. Lister, and Q. Li (2008). Urbanization effects in large-scale temperature records, with an emphasis on China. *Atmospheres*, 113, 122–133. 11
- Joseph, A., J.T. Odametey, E.K. Nkebi, A. Pereira, R.G. Prabhudesai, P. Mehra, A.B. Rabinovich, V. Kumar, S. Prabhudesai, and P. Woodworth

- (2006). The 26 December 2004 Sumatra tsunami recorded on the coast of West Africa. *Afr. J. Mar. Sci.*, 28, 705–712. 61, 66
- Kanamori, H., and Anderson D. L. (1975). Amplitude of the earth's free oscillations and long-period characteristics of the earthquake source. *J. Geophys. Res.*, 80, 8. 69
- Karl, T. R., and K. E. Trenberth (2003). Modern Global Climate Change. *Science*, 302, 1719–1723. 9, 10
- Keeling, C. D., J. F. S. Chin, and T. P. Whorf (1996). Increased activity of northern vegetation inferred from atmospheric CO₂ measurements. *Nature*, 382, 146–149. 10
- Király, A., and I. M. Jánosi (2005). Detrended fluctuation analysis of daily temperature records: Geographic dependence over Australia. *Meteorol. Atmos. Phys.*, 88, 119. 27, 34, 35, 37, 40
- Király, A., I. Bartos and I.M. Jánosi (2006). Correlation properties of daily temperature anomalies over land. *Tellus*, 58A, 593. 26, 27
- Koscielny-Bunde, E., A. Bunde, S. Havlin, H.E. Roman, Y. Goldreich and H.-J. Schellnhuber (1998). Indication of a Universal Persistence Law Governing Atmospheric Variability. *Phys. Rev. Lett.*, 81, 729–732. 26, 27, 34, 45
- Kurnaz, M. L. (2004). Detrended fluctuation analysis as a statistical tool to monitor the climate. *J. Stat. Mech.*, P07009. 26
- Lambeck, K. (1988). Geophysical Geodesy, The Slow Deformations of the Earth. Oxford Science Publications, Oxford (UK). 61
- Lanfredi, M., T. Simoniello, V. Cuomo and M. Macchiato (2009). Discriminating low frequency components from long range persistent fluctuations in daily atmospheric temperature variability *Atmos. Chem. Phys.*, 9, 4537. 27, 34
- Laurenza, M., A. Vecchio, Storini M. and Carbone V.(2012), Quasi-biennial Modulation of Galactic Cosmic Rays, *ApJ*, 749, 167. 46, 71
- Leith, C. E. (1973). the Standard Error of Time-Average Estimates of Climatic Means. *J. Appl. Meteorol.*, 12, 1066–1069. 49
- Liu, Y., and R. Avissar (1999). A study of persistence in the land-atmosphere system using a general circulation model and observations. *Journal of Climate*, 12, 2154–2168. 27
- Loh, C. H., T. C. Wu, and N. E. Huang (2001), Application of the empirical mode decomposition-Hilbert spectrum method to identify near-fault

BIBLIOGRAPHY

- ground-motion characteristics and structural response, *B. Seismol. Soc. Am.*, *91*, 1339–1357. 45, 71
- Loreto, V., G. Paladin, M. Pasquini, and A. Vulpiani (1996). Characterization of chaos in random maps. *Physica A Statistical Mechanics and its Applications*, *232*, 189–200. 20
- Lu, Q., R. Lund, and L. Seymour (2005). An Update of U.S. Temperature Trends, *J. Climate*, *18*, 4906–4914. 45, 51, 55
- Lund, R., Seymour, L. and Kafadar, K. (2001). Temperature trends in the United States. *Environmetrics*, *12*, 673–690. 51, 55
- Maas, L. R. M. (1997). On the nonlinear Helmholtz response of almost-enclosed tidal basins with a sloping bottom. *J. Fluid Mech.*, *349*, 361. 68
- Mann, M. E., J. Park, and R. S. Bradley (1995). Global interdecadal and century-scale climate oscillations during the past five centuries. *Nature*, *378*, 266. 10, 21, 26
- Mann, M. E. and J. Park (1996). Greenhouse warming and changes in the seasonal cycle of temperature: Model versus observations. *Geophys. Res. Lett.*, *23*, 1111–1114. 10, 21, 26
- McKinnell, S. M., and W. R. Crawford. The 18.6-year lunar nodal cycle and surface temperature variability in the northeast Pacific. *Journal of Geophysical Research (Oceans)*, *112*, 2002–2016. 18, 23
- Melini, D., and A. Piersanti (2006). Impact of global seismicity on sea level change assessment. *J. Geophys. Res.*, *111*, B03406. 61, 68
- Menne, M. J., C. N. Williams, and R. S. Vose (2009). The U.S. Historical Climatology Network Monthly Temperature Data, Version 2 *B. Am. Meteorol. Soc.*, *90*, 993–1007. 45
- Merrifield, M. A., et al. (2005). Tide gauge observations of the Indian Ocean tsunami, December 26, 2004. *Geophys. Res. Lett.*, *32*, L09603. 61
- Monetti, R. A., S. Havlin and A. Bunde (2003). Long-term persistence in the sea surface temperature fluctuations. *Physica A*, *320*, 581. 26, 39
- Muller, R., A. Dollfus, M. Montagne, J. Moity, and J. Vigneau (2000). Spatial and temporal relations between magnetic elements and bright points in the photospheric network. *A&A*, *359*, 373–380. 58
- Ott, E. (2002). *Chaos in Dynamical Systems*. Cambridge Univ. Press, New York, 2002. 18, 20

-
- Parker, D. E. (2006). A Demonstration That Large-Scale Warming Is Not Urban. *J. clim.*, 19, 2882–2895. 11
- Peng, C. K. et al. (1994). Mosaic organization of DNA nucleotides. *Phys. Rev. E*, 49, 1685–1689. 26
- Peterson, T. C. (2003). Assessment of Urban Versus Rural In Situ Surface Temperatures in the Contiguous United States: No Difference Found. *J. clim.*, 16, 2941–2959. 11
- Pezzulli, S., D. Stephenson, and A. Hannachi (2005). The variability of seasonality. *J. clim.*, 18, 71–88. 9, 17
- Platt, N., E. A. Spiegel, and C. Tresser (1993). On-off intermittency - A mechanism for bursting. *Phys. Rev. Lett.*, 70, 279–282. 20
- Rasmusson, E. M., and T. H. Carpenter (1983). The relationship between eastern equatorial Pacific sea surface temperatures and rainfall over India and Sri Lanka. *Mon. Wea. Rev.*, 111, 517–528. 38
- Rind, D. (2002). The Sun’s Role in Climate Variations. *Science*, 296, 673–678. 10
- Robinson, P. M. (2003). Long-memory time series. *Time Series with Long Memory*. Eds. P. M. Robinson, Oxford University Press, 382pp. 47
- Ropelewski, C. F., and M. S. Halpert (1989). Precipitation patterns associated with the high index phase of the Southern Oscillation. *J. Climate*, 1, 172–182. 38, 39, 41
- Royer, T. C. (1993). High-latitude oceanic variability associated with the 18.6-year nodal tide. *J. Geophys. Res.*, 98, 4639–4644. 18, 23
- Santer, B. D., T. M. L. Wigley, J. S. Boyle, D. J. Gaffen, J. J. Hnilo, D. Nychka, D. E. Parker, and K. E. Taylor (2000). Statistical Significance of Trends and Trend Differences in Layer-Average Atmospheric Temperature Time Series. *J. Geophys. Res.*, 105, 7337–7356. 44
- Santer, B. D., P. W. Thorne, L. Haimberger, K. E. Taylor, T. M. L. Wigley, J. R. Lanzante, S. Solomon, M. Free, P. J. Gleckler, P. D. Jones, T. R. Karl, S. A. Klein, C. Mears, D. Nychka, G. A. Schmidt, S. C. Sherwood and F. J. Wentz (2008). Consistency of modelled and observed temperature trends in the tropical troposphere. *Int. J. Climatol.*, 28, 1703–1722. 44
- Scafetta, N., and B.J. West (2003). Multiscaling comparative analysis of time series and a discussion on "earthquake conversations" in California. *Phys. Rev. Lett.*, 90, 248701. 26

BIBLIOGRAPHY

- Scafetta, N., and B. J. West (2008). Is climate sensitive to solar variability?. *Physics Today*, 61, 50–51. 10
- Stine, A. R., P. Huybers, and I. Y. Fung (2009). Changes in the phase of the annual cycle of surface temperature. *Nature*, 457, 435–440. 9, 10, 21, 28
- Stoev, S., and M. R. Taqqu (2004). Simulation methods for linear fractional stable motion and FARIMA using the fast Fourier transform. *Fractals*, 12, 95–121. 47
- von Storch, H., and F. Zwiers (1999). *Statistical Analysis in Climate Research*, Cambridge University Press. 47
- Syroka, J., and R. Toumi (2001). Scaling and persistence in observed and modelled surface temperature. *Geophys. Res. Lett.*, 28, 3255–3258. 26, 27
- Talkner, P., and R.O. Weber (2000). Power spectrum and detrended fluctuation analysis: Application to daily temperatures. *Phys. Rev. E*, 62, 150–160 (2000). 34
- Terradas, J., R. Oliver, and J. L. Ballester (2004). Application of Statistical Techniques to the Analysis of Solar Coronal Oscillations *Astrophys. J.*, 614, 435. 64
- The Royal Society (2010), *Climate change: a summary of the science*. 43
- Thomson, D. J. (1995). The Seasons, Global Temperature, and Precession, *Science*, 268, 59–68. 9, 10, 16, 21, 28
- Thomson, D. J. (1997). Dependence of Global Temperatures on Atmospheric CO₂ and Solar Irradiance. *Proceedings of the National Academy of Science*, 94, 8370–8377. 9, 10
- Titov, V., A. B. Rabinovich, H. O. Mofjeld, R. E. Thomson, and F. I. González (2005). The global reach of the 26 December 2004 Sumatra tsunami. *Science*, 23, 2045. 61
- Vecchio, A., and V. Carbone (2010). Amplitude-frequency fluctuations of the seasonal cycle, temperature anomalies, and long-range persistence of climate records. *Phys. Rev. E*, 82 66101–66108. 13, 26, 28, 30, 35, 40
- Vecchio, A., V. Capparelli, and V. Carbone (2010), The complex dynamics of the seasonal component of USA’s surface temperature, *Atmos. Chem. Phys.*, 10, 9657–9665. 28, 30, 31, 40, 46, 71
- Vecchio, A., M. Laurenza, V. Carbone, and M. Storini (2010). Quasi-biennial Modulation of Solar Neutrino Flux and Solar and Galactic Cosmic Rays by Solar Cyclic Activity. *Astrophys. J.* 709, L1. 30, 64

- Vecchio, A., M. Anzidei, V. Capparelli, V. Carbone, and I. Guerra (2012). *Has the Mediterranean Sea felt the March 11th, 2011, Mw 9.0 Tohoku-Oki earthquake?*. *EPL* 98, 59001. 69
- Vyushin, D., I. Zhidkov, S. Havlin, A. Bunde and S. Brenner (2004). *Volcanic forcing improves atmosphere-ocean coupled general circulation model scaling performance*. *Geophys. Res. Lett.*, 31 L10206. 27
- Wallace, C. J. and T. J. Osborn (2002). *Recent and future modulation of the annual cycle*. *Climate Research*, 22, 1–11. 10, 21, 28
- Weber, R. O. and P. Talkner (2001). *Spectra and correlations of climate data from days to decades*. *J. Geophys. Res.*, 106, 20131–20144. 37
- Wilson, R., G. Wiles, R. D’Arrigo, and C. Zweck (2007). *Cycles and shifts: 1,300 years of multi-decadal temperature variability in the Gulf of Alaska*. *Climate Dynamics*, 28, 425–440. 17, 23
- Woodworth, P. L., D. L. Blackman, P. Foden, S. Holgate, K. Horsburgh, P. J. Knight, D. E. Smith, E. A. Macleod, and E. Bradshaw (2005). *Evidence for the Indonesian Tsunami in British tidal records*. *Weather*, 60, 263–267. 61
- Woodworth, P. L., T. Aarup, and W. S. Wilson (2010). *Understanding sea level rise and variability*. Blackwell Publishing, New York (USA). 61
- Wu, Z. and N. E. Huang (2004). *A study of the characteristics of white noise using the empirical mode decomposition method*. *Royal Society of London Proceedings Series A*, 460, 1597–1611. 11, 12, 29, 47, 64
- Wu, Z., N. E. Huang, S. R. Long, and C. K. Peng (2007). *On the trend, detrending, and variability of nonlinear and nonstationary time series*, *Proc. Nat. Acad. Sci.*, 104, 14889–14894. 44, 46, 55
- Wu, Z., E. Schneider, B. Kirtman, E. Sarachik, N. Huang, and C. Tucker (2008). *The modulated annual cycle: an alternative reference frame for climate anomalies*. *J. clim.*, 31, 823–841. 13, 28, 30, 40
- Wu, Z., and N. E. Huang (2009). *Ensemble Empirical Mode Decomposition: a Noise-Assisted Data Analysis Method*. *Advances in Adaptive Data Analysis*, 1, 1–41. 13, 31
- Wunsch, C., and D. Stammer (1997). *Atmospheric loading and the oceanic “inverted barometer” effect*. *Reviews of Geophys.*, 35, 79. 62
- Yasuda, I., S. Osafune, and H. Tatebe (2006). *Possible explanation linking 18.6-year period nodal tidal cycle with bi-decadal variations of ocean and climate in the North Pacific*. *Geophys. Res. Lett.*, 33, L8606–L8609. 23

BIBLIOGRAPHY

Yndestad, H. (2006). *The influence of the lunar nodal cycle on Arctic climate.* *J. Mar. Sci.*, 63, 401–420. 16

Zhen-Shan, L., and S. Xian (2007). *Multi-scale analysis of global temperature changes and trend of a drop in temperature in the next 20 years.* *Meteorol. Atmos. Phys.*, 95, 115.

